UNIVERSITAT POLITÈCNICA DE CATALUNYA
BARCELONATECH
Escola d'Enginyeria de Barcelona Est

BACHELOR THESIS

Chemical Engineering Degree

Treatment of Acide Mine Drainage (AMD) containing rare earth element, by ceramic nanofiltration membrane

TFG memoir

Author: Ricardo Pirabed AGBOGLADJA
Director: Oriol Gibert Agulló
Supervisor: Julio López Rodríguez
Convocation: October 2018

ABSTRACT

Acid Mine Drainage (AMD) often emerges naturally, however the extraction activities in the mine industry have recently increased the influence of different chemical, physical and biological factors related to its production. Hence, the activity of humans is again the main protagonist if the intensification of AMD negative impacts on water sources, plants and animals. Generally, AMD is produced by the oxidative dissolution of sulphide minerals producing a drainage with low pH and high concentration in sulphate, heavy metals such as (iron, copper, zinc, lead) and others rare earth elements (REE) like (lanthanum, ytterbium and neodymium). Within this context, this project aims to extend the application of nanofiltration (NF) on AMD treatment using ceramic membranes. In this case AMD treatment can be understood as a procedure aims to reduce the amount of sulphate, aluminium, iron and REE among others elements present in an AMD solution by NF technique. Primarily the performance of NF oxide titanium [TiO2] membrane was used to study the rejection of dominant salts, aluminium and iron sulphate, at pH (1 and 1.5) and different concentrations with a synthetic solution that reproduces AMD solutions. Others traces ions such as zinc, copper, calcium and REE were also combined into that solution to study their rejection under the influence of the dominant salts previously introduced. The experiments were performed in a lab-scale installation, where, the concentrations vary from 300 to 1900 ppm for aluminium and from 500 to 2000 ppm for iron on one hand. On the other, REE concentrations were maintained constant at a nominal concentration of 10 ppm. Consecutively, the experimental data were fitted by means of the solution-diffusion-film-model (SDFM) in order to calculate the membrane permeabilities to each ion. This document, firstly starts with the introduction that explores all the basic concepts to understand the mechanics of NF. Secondly, the objectives and the methodology explain the steps to achieve the objectives proposed. Finally the results analysis, cost evaluation and the environmental impact sections pretend to give strength to all the key aspects investigated.

ACKNOWLEDGEMENTS

This project was carried out within the framework of the final academic project in chemical engineering degree. It was made possible by different people who directly and indirectly collaborated with great interest on the subject. For that reason, I gratefully acknowledge all of them and in special the help of my supervisors Oriol Gibert and Julio López, as well as the collaboration of my honourable friend Georgina Menchón and finally to my family who gave me all the necessary support to achieve these goals.

GLOSSARY – ACRONYMS

AMD Acid Mine Drainage.

CM Ceramic membranes.

CPL Concentration Polarization Layer.

DE Donnan Exclusion.

DiE Dielectric Exclusion.

HM Heavy Metals.

HTM Hollow Tubular Module.

ICP Inductively Coupled Plasma.

IEP Iso-Electric Point.

Kw Hydraulic permeability.

MF Microfiltration.

NF Nanofiltration.

PFM Plate-and-Frame Module.

REE Rare Earth Element.

RO Reverse Osmosis.

SDFM Solution-Diffusion-Film-Model.

SWM Spiral Wound Module.

TMP Trans-membrane-pressure.

UF Ultrafiltration.

GLOSSARY – NOTATION

$\mathbf{Z}_{+/-}$ Ion charge [+ / −].

$\mathbf{Z}_t$ Charge of trace ion [+ / −].

δ Concentration-polarization layer thickness [m].

$\mathbf{D}_{+/-,\mathbf{s}}{}^{\delta}$ Diffusion coefficient [$\mathrm{m}^2 \cdot \mathrm{s}^{-1}$].

$\mathbf{D}_s{}^{\delta}$ Diffusion coefficient of dominant salt [$\mathrm{m}^2 \cdot \mathrm{s}^{-1}$].

$\mathbf{D}_t{}^{\delta}$ Diffusion coefficient of trace ion [$\mathrm{m}^2 \cdot \mathrm{s}^{-1}$].

$\mathbf{P}_s$ Membrane permeability to dominant salt [$\mathrm{m} \cdot \mathrm{s}^{-1}$].

$\mathbf{P}_s{}^{\delta}$ Concentration-polarization layer permeability to dominant salt [$\mathrm{m} \cdot \mathrm{s}^{-1}$].

$\mathbf{Pe}_s$ Peclet number of dominant salt.

$\mathbf{Pe}_t$ Peclet number of trace ion.

$\mathbf{P}_{+/-}$ Membrane permeability to single ion [$\mathrm{m} \cdot \mathrm{s}^{-1}$].

$\mathbf{P}_t$ Membrane permeability to trace ion [$\mathrm{m} \cdot \mathrm{s}^{-1}$].

$\mathbf{R}_s{}^{\mathbf{Obs}}$ Observable rejection of dominant salt [%].

$\mathbf{R}_s{}^{\mathbf{Int}}$ Intrinsec rejection of dominant salt [%].

$\mathbf{R}_t{}^{\mathbf{Int}}$ Intrinsec rejection of trace ion [%].

$\mathbf{f}_t$ Reciprocal intrinsec trans-membrane passage of trace ion[%].

$\mathbf{f}_s$ Reciprocal intrinsec trans-membrane passage of dominant salt[%].

$\mathbf{C}_s{}^{"}$ Solute concentration in permeate stream [$\mathrm{mol} \cdot \mathrm{m}^{-3}$].

$\mathbf{C}_s{}^{'}$ Solute concentration in feed solution [$\mathrm{mol} \cdot \mathrm{m}^{-3}$].

$\mathbf{C}_s{}^{m}$ Solute concentration at membrane surface [$\mathrm{mol} \cdot \mathrm{m}^{-3}$].

$\mathbf{C}_t{}^{m}$ Trace ion concentration at membrane surface [$\mathrm{mol} \cdot \mathrm{m}^{-3}$].

$\mathbf{C}_t{}^{'}$ Trace ion concentration in feed solution [$\mathrm{mol} \cdot \mathrm{m}^{-3}$].

$\mathbf{C}_t{}^{"}$ Trace ion concentration in permeate [$\mathrm{mol} \cdot \mathrm{m}^{-3}$].

Contents

Chapter 1

INTRODUCTION

1.1 Acid mine drainage

The mining industry has a notable impact on the modern life and widely influences some well-known technologicals application and developments. Recent works and new methods have led to improve the supply for the growing demand on raw material like gold, copper, nickel and other important elements. However, the extracting activities under uncontrolled and non-regulated conditions generate different threats for the aquatic environment in proximity to the mine site. In this context, Acid Mine Drainage (AMD) mainly refers to the water produced from mining processes which is often harmful for the environment. The susceptible areas to the major impacts are rivers, groundwater, lakes and coastal waters. When AMD are discharged without the adequate treatment and canalisation, they increasingly become a complex source of long-term impairment to waterways and biodiversity. Different studies have described AMD as multi-factor pollutant and introduced different approaches to prevent and attenuate their negative impact. As reported by Akcil et al. [1], AMD is an important environmental disaster that can be solved actively using filtration technology.

Generally, AMD are formed when metal-sulphide minerals, table 1.1, are exposed to oxygen and water or to a humid environment. The main metal-sulphide minerals responsible for AMD generation are the ones containing iron (pyrite and marcasite). Although any mineral with sulphide is a potential source of AMD and the exposure to them is more important in certain activities than others.

Metal sulphide	Chemical formula
Pyrite	FeS_2
Marcasite	FeS_2
Pyrrhotite	$Fe_{1-x}S$
Chalcocite	Cu_2S
Covelite	CuS
Chalcopyrite	$CuFeS_2$
Molybdenite	MoS_2
Millerite	NiS
Galena	PbS
Sphalerite	ZnS
Arsenopyrite	FeAsS

Table 1.1: *Different metal-sulphide minerals that contribute to AMD generation, [2]*

As shown in table 1.2, the primaries sources like underground and open pit mine adding to construction rock are scenario where AMD has gained a considerable weight due to the possibility to be directly in contact with large amount of water. Therefore, AMD can occur where any sulphide materials are exposed. In general, any activities that disturb sulphide minerals can lead to AMD as it is already shown in table 1.2.

Primary sources	Secondary sources
❑ Mine rock dumps	❑ Treatment sludge pounds
❑ Tailings impoundment	❑ Rock cuts
❑ Underground and open pit mine workings	❑ Concentrated load-out
❑ Pumped/nature discharged underground water	❑ Stockpiles
❑ Diffuse seeps from replaced overburden in rehabilitated areas	❑ Concentrate spills along roads
❑ Construction rock used in roads, dams, etc.	❑ Emergency ponds

Table 1.2: *Primary and secondary source of AMD, [1]*

The chemistry behind AMD generation is well-known. However, the level of pollution depends on various factors, such as the chemical composition of the mining site, the presence of micro-organisms, temperature, water and oxygen availability. These variables vary from one area to another, for that reason, more important studies need to be performed to clarify their correlation with AMD generation and their contribution to the negative impacts. According to Simate et al. [2], it has become clear that the threat of AMD to the environment will not be solved in the short to medium term, and not by a single intervention, but will rather require the integrated implementation of a range of measures and processes. So, there is a tremendous and urgent need for further research and innovation in order to develop new separation and purification technologies.

1.1.1 AMD generation

As it has been mentioned, the main origin of AMD is the oxidation of metal-sulphides. According to [1], the most important reaction is the oxidation of pyrite, as exemplified in the following reactions.

$$2\,FeS_{2(s)} + 7\,O_2 + 2\,H_2O \longrightarrow 2\,Fe^{2+} + 4\,{SO_4}^{2-} + 4\,H^+ \quad \{1\}$$

The rate of pyrite oxidation depends on the solid phase composition and the availability of oxygen and water. So, the products from reaction (1) represent an increase in the total ferrous ions Fe^{2+}, sulphate ${SO_4}^{2+}$ and acidity. As stated in [2], some environmental factors such as oxygen O_2 concentration, pH (when greater than 3.5) and bacterial activity lead ferrous ions to oxidise to ferric ions Fe^{3+} as shown in reaction (2).

$$Fe^{2+} + \frac{1}{4}\,O_2 + H^+ \xleftrightarrow{pH > 3.5} Fe^{3+} + \frac{1}{2}\,H_2O \quad \{2\}$$

When the concentration of oxygen decreases, reaction (2) will not occur until the pH reaches 8.5, [1]. Therefore, in many cases, reaction (2) rate controls pyrite oxidation because of the lower conversion of ferrous oxidation at pH below 5 in abiotic condition. In addition to that,

when pH is between 2.3 and 3.5, most of the ferric ions generated in reaction (2) precipitate to ferrous hydroxide $Fe(OH)_3$, as described in reaction (3).

$$Fe^{3+} + 3\,H_2O \xrightarrow{pH = 2.3 - 3.5} Fe(OH)_3\downarrow + 3\,H^+ \quad \{3\}$$

Furthermore, any ferric ions Fe^{3+} from reaction (2) that do not precipitate in addition with those obtained from hydroxide dissosiation at pH 2 will oxidise more quantity of pyrite, according to reaction (4), [1].

$$FeS_{2(s)} + 14\,Fe^{3+} + 8\,H_2O \longrightarrow 15\,Fe^{2+} + 2\,{SO_4}^{2-} + 16\,H^+ \quad \{4\}$$

The global reaction (5) combines reactions (1,2 and 3) and outlines the first step in pyrite dissociation as well as ferric ions precipitation as $Fe(OH)_3$.

$$FeS_{2(s)} + \frac{15}{4}\,O_2 + \frac{7}{2}\,H_2O \longrightarrow Fe(OH)_3\downarrow + 2\,{SO_4}^{2-} + 4\,H^+ \quad \{5\}$$

However, the overall reaction for stable ferric iron that oxidises additional pyrite in combination with reaction (5) is over viewed in global reaction (6).

$$FeS_{2(s)} + \frac{15}{8}\,O_2 + \frac{13}{2}\,Fe^{3+} + \frac{17}{4}\,H_2O \longrightarrow \frac{15}{2}\,Fe^{2+} + 2\,{SO_4}^{2-} + \frac{17}{2}\,H^+ \quad \{6\}$$

All that said, the presence of iron is an important factor in the generation of AMD and its identification as explained in the previous reactions. In this context the identification of AMD refers to the red-orange colour that often indicates the presence of iron in the effluents. Nevertheless, there are other metal-sulphides listed in table 1.1 that involve other metals such as Zn; Cu; Cd; As; Ni; Pb, whose dissociation follows a similar reaction mechanism.

1.1.2 AMD impact

The presence of AMD is characterized by several factors, which can pose severe environmental problems when it flows into groundwater, streams and rivers. The important factors, among others, are high concentration of sulphate, acid pH and the presence of Heavy Metals (HM). Therefore, AMD is very toxic to aquatic organisms and destroys the ecosystems around. It also, corrodes the infrastructures nearby and taints water in regions where potable source is already a scarcity. The effects of HM from AMD on human health and plants as well as the negative impact of acidic pH on aquatic life will be the main subject of this part.

HM refers to elements with atomic density greater than 6 g/cm^3 or conventionally to those with metallic properties and with the atomic number greater than 20. Their negative impact on human and animal health is notable due to their long term accumulation in the organisms with the related toxicity. Regarding humans and animals health, HM can harm in two aspects. Firstly, they have the ability to persist in natural ecosystems for an extended period of time. Secondly, they have the ability to accumulate in successive levels of the biological chain, causing severe and chronic diseases. Generally, HM poisoning leads to malfunction of metabolic mechanisms. They also disrupt the metabolic functions by accumulating in vital organs and glands such as the heart, brain, kidneys, bones and liver. Adding to that, they inhibit the absorption and displace the vital nutritional minerals far away from the electric equilibrium, thereby, hindering biological functions. A brief summary of some important HM and their effects on human health together with permissible level are listed in table 1.3.

Heavy metal	Effect	Permissible level (mg/L)
Arsenic	Bronchitis, dermatitis, poisoning	0.02
Cadmium	Renal dysfunction, lung disease, lung cancer, bone defects, increased blood pressure, kidney damage, bronchitis, bone marrow cancer, gastrointestinal disorder	0.06
Lead	Mental retardation in children, developmental delay, fatal infant encephalopathy, congenital paralysis, sensor neural deafness, liver, kidney, and gastrointestinal damage, acute or chronic damage to the nervous system, epilepticus	0.10
Manganese	Inhalation or contact causes damage to nervous central system	0.26
Mercury	Damage to the nervous system, protoplasm poisoning, spontaneous abortion, minor physiological changes, tremors, gingivitis, acrodynia characterized by pink hands and feet	0.01
Zinc	Damage to nervous membrane	15.0
Chromium	Damage to the nervous system, fatigue, irritability	0.05
Copper	Anaemia, liver and kidney damage, stomach and intestinal irritation	0.10

Table 1.3: *HM impact on human health and permissible limit, [2]*

Furthermore, soil contamination by HM is a critical environmental crisis due to their potential adverse ecological effects. High concentrations and/or certain mixtures of HM like cadmium in plant tissues can disturb the growth in different ways. Studies reveal that different family of plants experience oxidative stress upon the exposure to zinc and chromium. This fact leads to cellular malfunction and disturbance of cellular ionic homoeostasis and consequently disrupting the physiology and morphology of vegetal life. Table 1.4 outlines the effect of different HM on plants, [2].

Heavy metal	Effects
Cadmium	Decreases seed germination, lipid content, and plant growth; induces phytochelatins production
Lead	Reduces chlorophyll production and plant growth; increases superoxide dismutase
Nickel	Reduces seed germination, dry mass accumulation, protein production, chlorophylls and enzymes; increases free amino acids
Mercury	Decreases photosynthetic activity, water uptake and antioxidant enzymes; accumulates phenol and proline
Zinc	Reduces Ni toxicity and seed germination; increases plant growth and ATP/chlorophyll ratio
Chromium	Decreases enzyme activity and plant growth; produces membrane damage, chlorosis and root damage
Copper	Inhibits photosynthesis, plant growth and reproductive process; decreases thylakoid surface area

Table 1.4: *HM impact on plant, [2]*

The pH of water is a fundamental factor in the aquatic life development, as it strongly, affects the physiological functions. That also includes the ions exchange phenomenon from water during the breathing process. However, such physiological processes, work normally in most aquatic ecosystems under a pH range varying from 6 to 9. Indeed, most of the freshwater lakes, streams, and ponds have a natural pH between 6 to 8. As result, when the pH exceeds the frame physiologically tolerated by the aquatic organisms it ends in numerous sub-lethal impacts, such as weak growth rate and premature mortality in some cases. The list of the negative influences of pH on aquatic life in different range, is shown in table 1.5.

pH	Effect
3.5–3.0	Toxic to most fish; some plants and invertebrates can survive such as the water bug, water boatmen and white mosses
4.0–3.5	Lethal to salmonids
4.5–4.0	Harmful to salmonids, tench, bream, roach, goldfish and the common carp; all stock of fish disappear because embryos fail to mature at this level
5.0–4.5	Harmful to salmonid eggs, fry and the common carp; the lake is usually considered dead and a “wet desert”; it is unable to support a variety of life
6.0–5.0	Critical pH level, when the ecology of the lake changes greatly; the number and variety of species begin to change; salmon, roach and minnow begin to become less diverse; less diversity in algae, zooplankton, aquatic insects, insect larvae; rainbow trout do not occur and molluscs become rare; there is a great decline in salmonid fishing; the fungi and bacteria that are important in organic matter decomposition are not tolerant so the organic matter degrades more slowly and valuable nutrients are trapped at the bed and are not released back into the ecosystem; most of the green algae and diatoms (siliceous phytoplankton) that are normally present disappear. The reduction in green plants allows light to penetrate further so acid lakes seem crystal clear and blue; snails and phytoplankton disappear
9.0–6.5	Harmless to most fish
9.5–9.0	Harmful to salmonids, harmful to perch if persistent
10.0–9.5	Slowly lethal to salmonids
11.0–10.5	Lethal to salmonids, carp, tench, goldfish and pike
11.5–11.0	Lethal to all fish

Table 1.5: *pH’s effects on aquatic life, [2]*

It also highlights that there is a gradual drawback as the pH values become further displaced from the normal range. For example, when the pH of most aquatic systems falls below 6 the ecology of the lake changes gradually and the number and variety of species begin to change. At pH close to 5, non-desirable species of plankton and mosses may begin to invade, and the population of fishes such as small-mouth bass disappears. Also, below pH 5, fish population begins to drop and the lake ground may be covered with necrotic material which increase mosses population near shore areas. To summarize, AMD negatively affects natural ecosystems such as aquatic life by varying the dissolved ions and salts present in its proximity, which is a disaster for the environment, [2].

1.2 Filtration technology

Inside the particle-fluid separation background, filtration generally refers to the act of separating, one or more, distinct phases or dissolved element from others by exploiting the physical and chemical differences. These differences, remain on physicochemical properties, such as, particle size, density, electric charge among others. However, the processes of filtration can be listed in two branches, solid-liquid and solid-gas separation. Indeed, these techniques aim to improve the requirements and qualities of products during manufacturing as well as the efficiency of the global process. For example, an important application in upstream of combustion, is the removal of solid contaminants from fuel or air to avoid damage in the engine. Adding to that, the removal of water in the process of sugar crystallization that avoids unnecessary costs in evaporation and transport. So, the use of filters fall into the removal of contaminants, from a valuable or useful fluid, for example their use in water treatment plants. All that said, this section aims to introduce the filtration technology.

1.2.1 General overview on membranes

In separation terms membrane is a thin, flexible and semi-permeable sheets of porous material, intended to separate species at the particle, molecular and ionic scales. A membrane is any material that, under the adequate operating conditions, is permeable to one or more components inside a solution or a suspension from a process stream, as reported in Chase et al. [3]. A scheme of a membrane separation process is shown in figure 1.1.

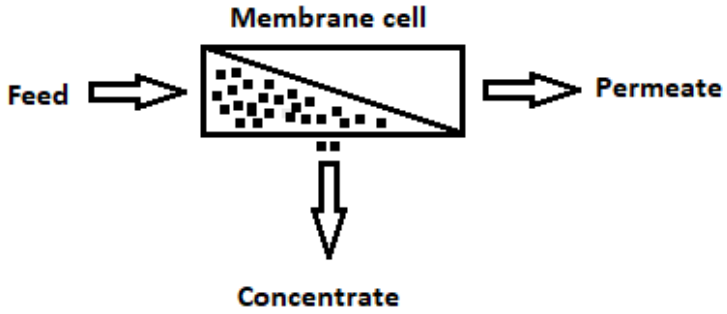

Figure 1.1: *Membrane symbol and nomenclature*

As shown, there are at least three streams for the filtration process. One as input,

that is commonly called feed, and two as outputs which are the concentrate and the permeate. The concentrate stream merges the different solutes rejected by the membrane and the permeate stream, has a low concentration of these solutes, comparatively to the feed solution.

However, as far is reasonable, a membrane should be strong, flexible, resistant to corrosion and abrasion and should be easily manipulated into the required shape. These requirements constraint sometime, the number of possible media, but still leave plenty of potential for new technique and material. Some examples are inorganic materials like minerals, carbon, glass, metals and metal oxides/ceramics besides organic materials from natural and synthetic source. Therefore, the membranes can be classified according to their main material and commercial format, as listed in table 1.6.

Material	Format
Carbon: natural activated	Granules or powder: loose, bonded, embedded Fibres: loose, felted, woven, embedded Porous block
Ceramics: metal oxides and others	Fibres and filaments: felted, woven, dry-laid (spun), Granules: loose, bonded, sintered , Wet-laid (paper, filter sheets), wet-laid (paper), rigidized, sintered Foam Extruded mesh ('Netlon') Sheet: perforated, stretched (fibrillated), porous, membrane
Processed natural fibre: Man-made organic: regenerated cellulose and synthetic polymers	Granules or powder: loose, sintered Formed blocks, with tubular holes Fibres: loose, sintered Foam

Table 1.6: *Membrane with their production materials and commercial format, [3]*

For industrial applications, membrane characterization is crucial in order to have a complete understanding on a filtration system. So, the performance delivers by a membrane can be tracked and studied. Therefore, in filtration applications were the pressure gradient is the driven force, variable like permeate flux and recovery, solute rejection and permeability are important to know. The flux in this context is the volume of permeate per membrane area and per unit of time; the rejection is the percentage of solute rejected from the feed stream; and, the permeability is the constant (K) that relates flux and Trans-membrane-pressure (TMP) defined by the equation (1.1).

$$J = K \cdot TMP \tag{1.1}$$

Hence, the membrane permeability to a solute/ion measures the easiness of being transported across the membrane. As a result, it is inversely proportional to the resistance presented by the membrane. Finally, permeate recovery is the fraction of feed that permeates through the membrane. A typical flow-pressure curve is shown in figure 1.2, is useful to know the membrane permeability for different solutions. Moreover, the permeability can be used as performance indicator, for example hydraulic permeability, labelled as Hydraulic permeability (Kw), was useful to know how flux variate during a cleaning operation in this project.

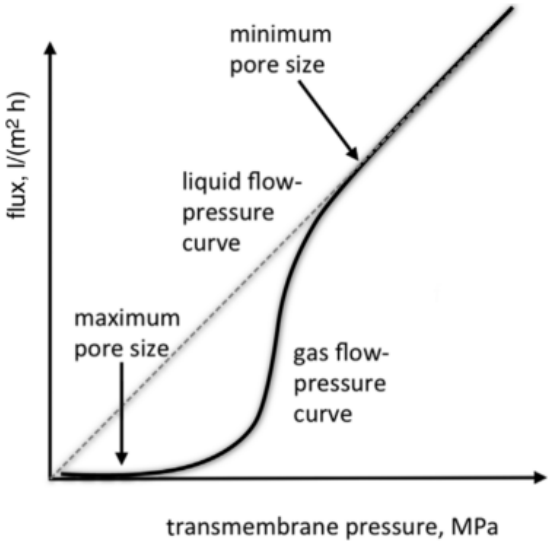

Figure 1.2: *Theoretical flow-pressure curve for gas and liquid, [4]*

1.2.2 Transport mechanism

The passage of solutes through a membrane can be described using the transport mechanism described in equation (1.2) and illustrated in figure 1.3, extracted from M.Yagnaseni et al. [5]. As observed, the flux of a solute is generated through the membrane by the transport with a concentration gradient and an electrostatic potential gradient. The electrical field is generated due to the difference between the coefficient diffusion of dominant salt ions, as reported in E. Yaroshchuk et al. [6]. In this project, the terms co-ions and counter-ions refer to the individual ionic elements that interact with the membrane charge. However co-ions will be used for the ions that have the same charge as the membrane and the counter-ions will indicate that the membrane and the ionic element have opposite charges.

$$J_i = J_v \cdot C_s^{"} = -D_i \cdot \left(\frac{dC_i}{dx} + Z_i \cdot C_i \frac{d\theta}{dx}\right) \tag{1.2}$$

where:
J_i: Trans-membrane flux of solute i $[mol \cdot m^{-2} \cdot s^{-1}]$
J_v: Volumetric trans-membrane flux $[m \cdot s^{-1}]$
$C_s^{"}$: Dominant salt concentration in permeate $[mol \cdot m^{-3}]$
D_i: Solute diffusion coefficient $[m^2 \cdot s^{-1}]$
dC_i/dx: Gradient concentration in membrane $[mol \cdot m^{-4}]$
C_i: concentration of solute i $[mol \cdot m^{-3}]$
Z_i: Charge of solute i
$d\theta/dx$: Electrostatic potential gradient $[m^{-1}]$

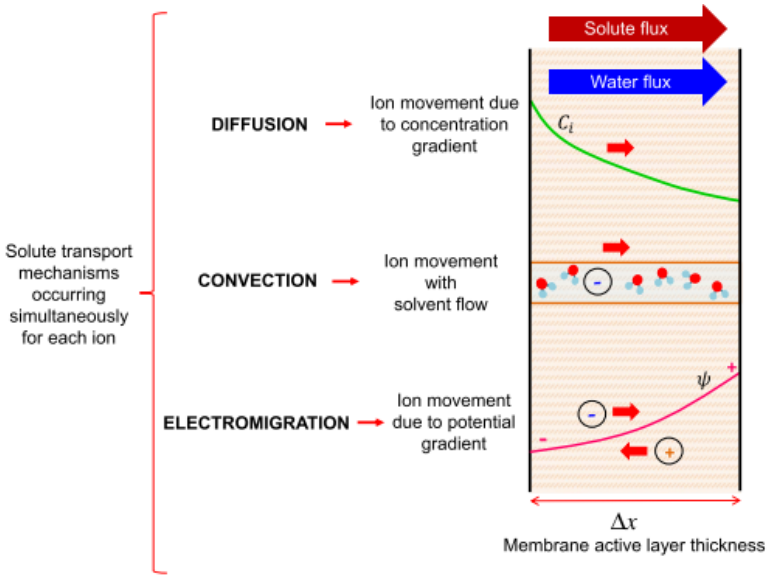

Figure 1.3: *General overview on solute transport mechanism, [5]*

1.2.3 Exclusion mechanisms

In addition to the transport mechanism previously introduced, the exclusion mechanisms generally complement the knowledge on the interactions between a membrane and a solute. The process inside a membrane can be widely described with three molecular scale phenomena, which are the size exclusion; Donnan Exclusion (DE) and Dielectric Exclusion (DiE) as reported in S. Park et al. [7]. Firstly, the size exclusion based on irreversible thermodynamics considers the membrane as a sieve which separates molecule by their size, without any consideration for the membrane electric properties. The others describe the solute transport as a function of the electrostatic interactions between the solute and the membrane. Moreover, the rejection mechanism due to the presence of the Concentration Polarization Layer (CPL) can be considered as transport phenomena as stated in Pages et al. [8]. In order to improve the capacity to predict Nanofiltration (NF) membrane behaviour, these mechanisms will be reviewed in the following parts.

Size exclusion

Physical sieving or size exclusion in filtration relies on the size of the solute and the pore dimension inside the membrane, as shown in figure 1.4. Consequently, the solutes with a size superior to the pore are rejected and then carried on the concentrate stream. It is useful to explain the rejection of colloids, large molecules and gases. Today is relatively easy to control the pore dimensions and shape in order to optimize the retention. Other porous materials can be made with polymeric matrix and active carbon as stated in Suda et al. [9]. In this case, the physical pore can be assimilated with a free volume, as at this scale they are not permanent and change during the operation.

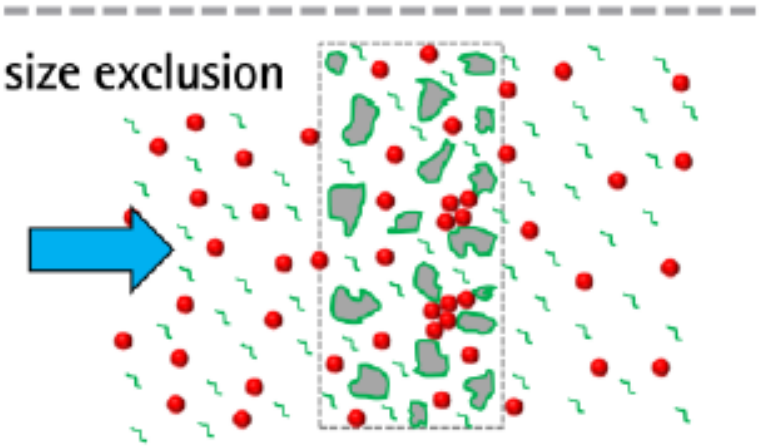

Figure 1.4: *Solute size exclusion in a nanofiltration process, [10]*

Donnan exclusion

DE, is also known as Gibbs-Donnan equilibrium and describes the behaviour of charged particles near a semi-permeable membrane that sometimes fail to distribute evenly across the two sides of the membrane. The presence of a charged group inside the membrane creates electrostatic attraction on the solute with opposite charge (counter-ions) and conversely generate repulsion on solute with the same charge (co-ions). For example A^+ and B^- are two charged solutes, as illustrated in figure 1.5, their rejection in both cases is controlled by the presence of a static third element $R^{-/+}$, which is a property of the membrane. Then, taking advantages from DE remains on the ability to control that property, which in occasion is a pH function. As some chemical groups such as carboxyl, nitrite can vary their charge depending on the pH. As result, some ionic species can pass through the membrane while others cannot, improving this way his performance which varies with the charge generate inside the membrane.

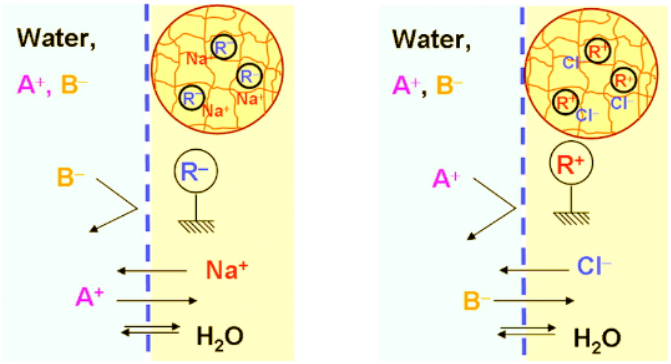

Figure 1.5: *Ions exclusion mechanism by Donnan effect inside a NF membrane, [11]*

Dielectric exclusion

DiE is caused by the interactions of ions with the bound electric charges induced by ions at interfaces between media of different dielectric constants. The pore geometry and solvent

dielectric constant are two important factors which affect the influence of DiE on solute exclusion. As shown in figure 1.6, the impact of DiE in an aqueous solution is the formation of a hydration shell around the ions which may help them to cross the membrane. Also, it appears that a fixed electric charge at the pore surface should give rise to the intensification of dielectric exclusion, as stated in [6].

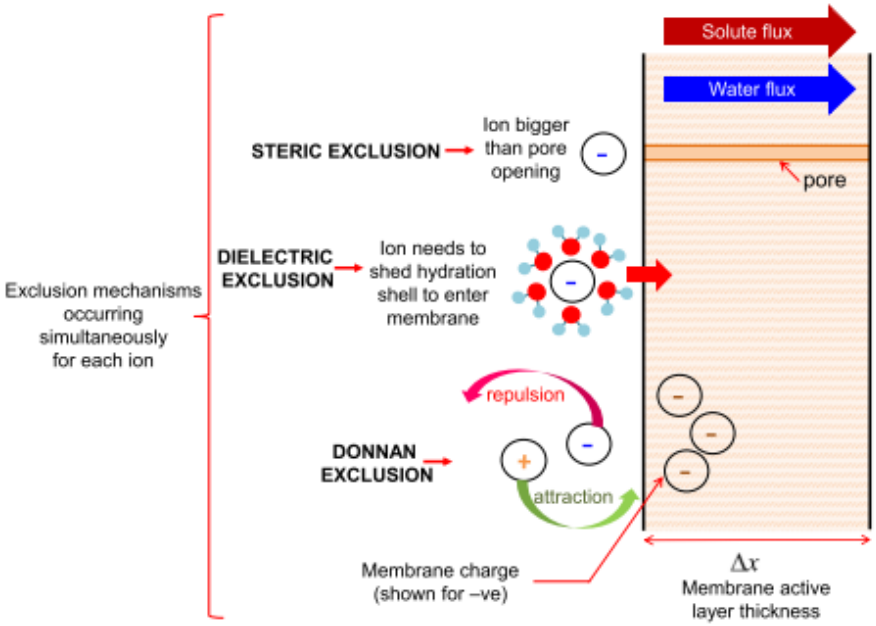

Figure 1.6: *General overview on exclusion mechanisms, [5]*

1.2.4 Concentration polarisation layer

Due to the differences between the coefficient diffusion of the different solutes present in a solution during the filtration process, the ions cross the membrane with different speed. Consequently, the superficial ions density at the feed side rises and then leading to the formation of CPL on the membrane, and simplified as CPL for the uses in this document. This exclusion mechanism is well-known for his contribution to explain the presence of concentration gradient. As shown in figure 1.7, this gradient controls the transport of ions by diffusion and electric migration. However, the role of convection needs to be studied.

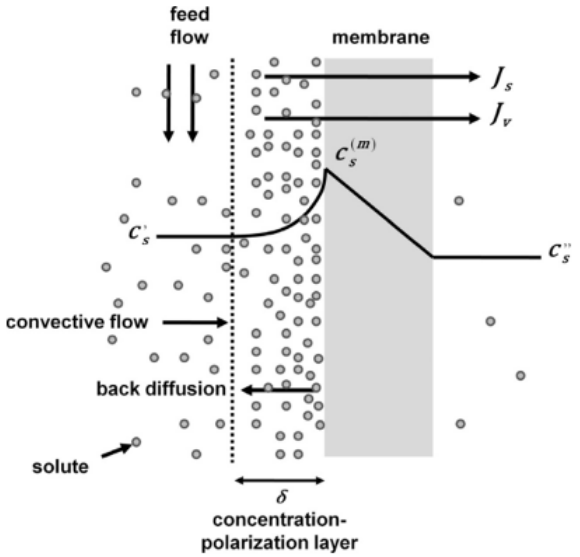

Figure 1.7: *Concentration polarization layer, [8]*

1.2.5 Nanofiltration

As outlined at the beginning of this section, the separation of solute from a liquid is an important area in filtration technologies and applications. Generally, a separation unit needs energy to transport fluid through the process. This is achieved in common application by applying different kinds of driven forces. As shown in figure 1.8 the most important forces are pressure, concentration and electric potential gradients. Consequently their effect are solute diffusion, static attraction-repulsion, electric migration and finally solute convection with the membrane.

Membrane Processes

Pressure Driven
- Reverse Osmosis (RO) → Diffusion
- Nano-filtration (NF) → Attraction/Repulsion
- Ultra-filtration (UF) → Diffusion/Convection
- Micro-filtration (MF) → Convection

Passive (Driving Force → *Concentration Gradient*)
- Dialysis (D) → Diffusion
- Gas Separation (GS) → Diffusion
- Pervaporation (PV) → Diffusion
- Liquid membrane (LM) → Diffusion

Electrically Driven (Driving Force → *Electrical Potential Gradient*)
- Electro-dialysis (ED) → Migration

Figure 1.8: *Membrane process with their driven force, [12]*

There are four types of operation for the pressure driven filtrations, Microfiltration (MF), Ultrafiltration (UF), NF and finally Reverse Osmosis (RO). As observed in figure 1.9, NF keeps the third position just after UF allowing to improve separation efficiency for multivalent ions and charged molecules.

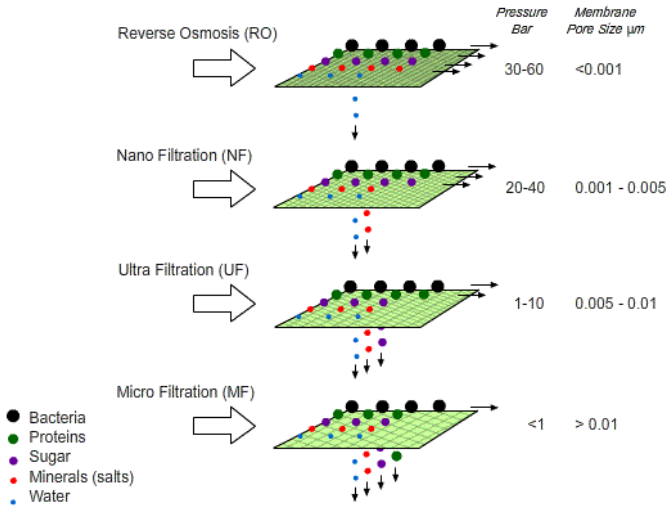

Figure 1.9: *Pressure driven filtration operations with their size separation, [12]*

NF technique has been firstly used for commercial purpose by the **FilmTec Corporation** (now Dow Chemical Company) in the mid-1980's to describe a new line of membrane, with properties between UF and RO. Since then, NF has found wide applications across a range of industrial sectors especially in water and waste-water treatment and desalination. Also, other applications include those in pharmaceutical, biotechnology, food and beverage. Moreover, the membranes used in NF have been improved during the last decades and still continue to capture the attention for their versatility as a separation tool. Currently, these membranes can have pore size or free-volume dimensions between 0.001 and 0.005 (μm) and can operate between 20 and 40 bar as observed in figure 1.9. Free-volume in NF membranes refers to the spontaneous holes created between the membrane material molecules that let the feed to flow. NF membrane can also exhibit positive or negative electrical charges due to the dissociation of functional groups or the adsorption of charged solutes as explained in Oatley-Radcliffe et al. [13] For example, polymeric NF membranes contain ionisable groups such as carboxyl and amine that could have positive or negative charge at diferent pH. Generally, NF membranes are negatively charged in neutral or alkaline conditions and positively charged in acidic condition according to J. Woei et al. [14]. Adding to that, the main transport mechanism in NF are diffusion and electric migration. However, convection can play a feeble role in occasion and finally, DE and DiE proved to be important exclusion mechanisms.

1.2.6 Membrane operation and module configuration

The dynamics of fluid is an important parameter to study for any membrane performance. The operation modes are divided in two categories: cross-flow and dead-end depending on the fluid flow direction according to the membrane active layer. Thus a well defined operation mode can prevent or reduce fouling in the membranes, which is their principal downside. Fouling in this context refers to the accumulation of solute and particles in/on a membrane, which happens inherently during any filtration process. Depending on their chemical characteristics fouling is classified in inorganic, organic, particulate and biologic. So, fouling depends on the feed quality and mainly on membrane characteristics as it has been reported in Nyström et al. [15]. The accumulation of solute on the membrane increases the resistance to the solution passage through

the active layer. For that reason, the efficiency during a filter performance can be demeaned. As a result, the removal of fouling with chemical or physical cleaning methods to restore the original properties of the membrane is very important and the price to pay for these properties recovery is membrane lifetime reduction.

In cross-flow configuration the feed flows tangentially to the membrane surface, as illustrated in figure 1.10 (top). This type of filtration is achieved by creating a positive pressure on the feed side, allowing a part of the feed to pass through the membrane as filtrate and retaining separated species inside the feed. That configuration increases the chance to remove trapped particles on the filters surface, as they are in constant contact with a stream, reducing thus membrane fouling. Nevertheless, cross-flow filtration uses more complex equipments, and is widely used in MF and UF where large volume of fluid with high viscosity and concentration in organic matter should be treated efficiently.

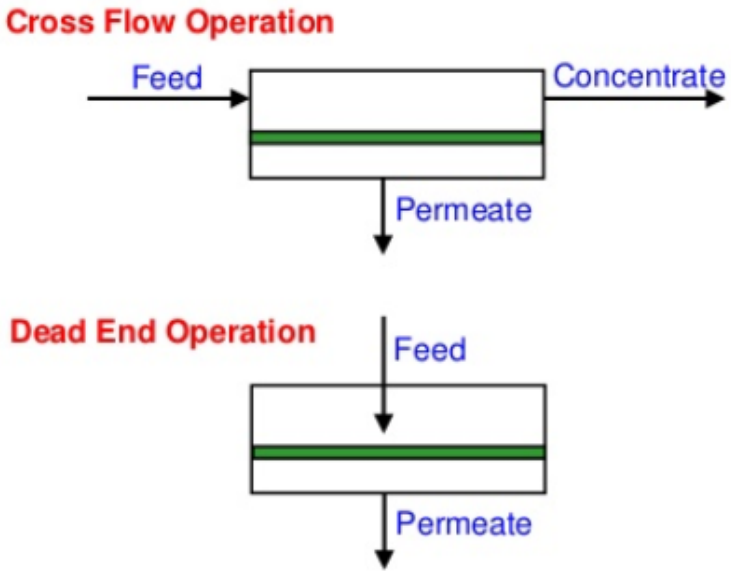

Figure 1.10: *Membrane operation in a cross-flow (top) and dead-end configuration (bottom), [16]*

Dead-end configuration set the feed to flow perpendicularly to the membrane, increasing in that way the contact between feed and the membrane surface, as shown in figure 1.10. The downside with this set-up is the accumulation of particles on membrane surface, thus increasing membrane fouling and leading to higher a demand in pressure to keep the permeate flux constant. The operations under dead-end filtration causes more fouling than in a cross-flow mode as reported in K. Sutherland et al. [17].

NF membrane are also packed in different modules to enhance permeate flux and solute rejection. Generally, there are three main configurations in NF that dominate the market, Plate-and-Frame Module (PFM), Spiral Wound Module (SWM) and Hollow Tubular Module (HTM).

The PFM module is the oldest configuration used in commercial applications and is made with multiple flat sheet packed together as a multi-layered sandwich. Each unit includes a support plate, a flat membrane sheet and spacers to distribute the feed flux over the membrane and improve mass transfer between the solution and the membrane.

The flat sheet placed on the permeate spacer is bent over the support plate, and then

forming an envelope opens to the feed from both sides. Also, the edges of the membrane are sealed to the support. Many of these units, called cassette, are stacked in parallel to create the module, as stated in [4], and illustrated in figure 1.12. The main advantages of PFM modules are the ease of cleaning, the replacement of defective membranes and adding to that, the ability to handle viscous feeds.

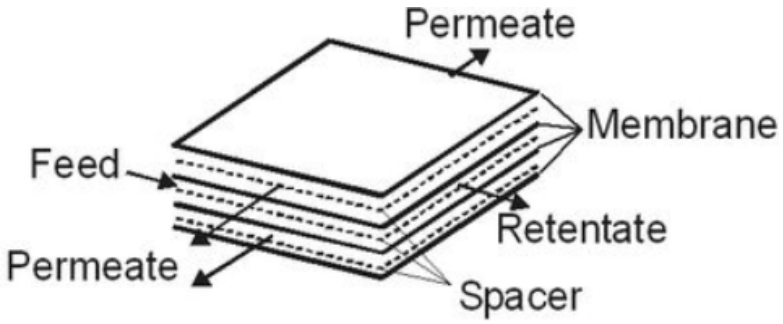

Figure 1.11: *Plate-and-Frame module structure, [18]*

The packing density of flat sheets is increased in SWM, invented few years after PFM modules. Consequently, the area per volume inside the cylinder shape container increase. The main advantages of the SWM are high packing density and their low manufacturing cost. In contrast, they present some complication during cleaning and maintenance task.

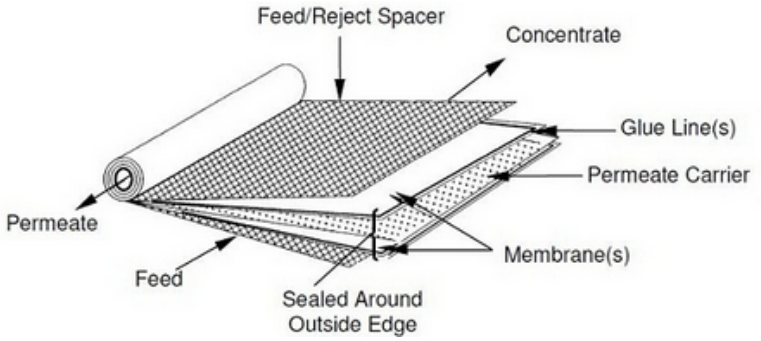

Figure 1.12: *Spiral wound module structure, [19]*

Finally, HTM embeds tubular membranes in a module similar to the one used for hollow fiber. They are bundled together inside a plastic or stainless steel vessel to form a cartridge, where they can be packed and then the packing density can be increased, due to the available area per volume. Usually, tubular module consist of several single tubular membranes with a diameter between 0.3 and 2.5 cm with a wall thickness of 2 mm. Tubular membranes can have either circular or elliptic cross sections, as shown figure 1.13a. Such membranes, are usually cast in place within a support tube made of fibreglass, ceramic, plastic or stainless steel to enhance higher mechanical strength, illustrates in figure 1.13b with membrane position highlighted in red. Moreover, the ease for cleaning and the replacement of damaged tube are the main advantage with HTM. Also, the tubes are also less prone to clogging than spirals. Finally, this option need high investment cost and large dead-end volume, which are its main drawbacks.

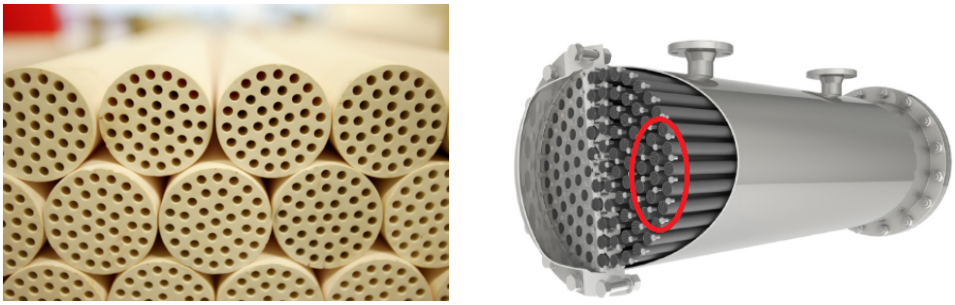

(a) *Tubular ceramic membrane*

(b) *Commercial ceramic module for water treatment*

Figure 1.13: *Single ceramic membrane and module for industrial applications, [14]*

1.2.7 Ceramics membrane synthesis

Although a variety of materials are being used through their complex production processes, many are still under investigation. The design of Ceramic membranes (CM) usually uses different elements with different size and shape as shown in figure 1.14. A strict definition of ceramics as inorganic non-metallic material prescribes the use of metal oxides or zeolites, and indeed alumina and silica are among the most common membrane precursors. The limited stability of the active layer in those membranes and the ongoing optimization led to the use of more stable (but also more expensive) material like titania (which is used in this project) and zirconia. Titanium dioxide (titania TiO_2 is a popular material used for CM coating, it is sought for its excellent chemical resistance at both acidic and alkali pH, as reported in [4].

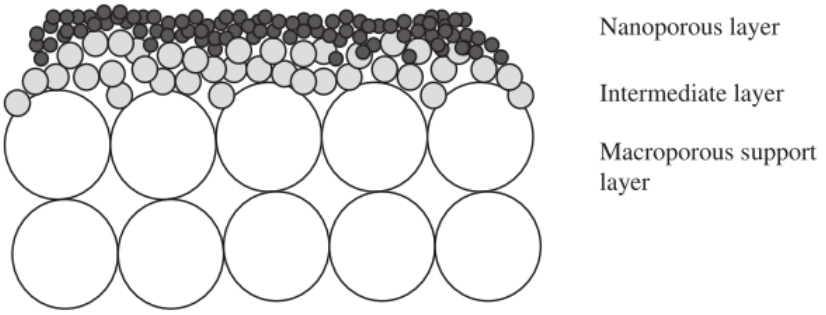

Figure 1.14: *Representation of ceramic asymmetric membrane derived from nanoparticle, [20]*

TiO_2 nano-particle CM based presents excellent chemical resistance, high water flux, photochemical and catalytic properties. As reported in J. Kim et al. [21], after a fabrication process carried out by Syafei in 2008, ATZ (alumina/ Titania / Zirconia) layer had been coated with TiO_2 nano-particles. In their study, an aqueous suspension containing 1.25 percent of Degussa P25 (about 80 percent anatase phase), 3.75 percent acetylacetone, and 5 drops of Triton X were stirred for 1 hour. The suspension was poured on top of the ATZ membrane positioned horizontally to ensure equal distribution of the solution on the membrane surface and temperature increased gradually to 450 °C. Sintering of metal oxide particles is the simplest approach to form a porous ceramic membrane and control the pore size. The pore size can be limited to the sizes

of ceramic precursors prior to the sintering stage. It has been reported that the pore size of TiO_2 nano-particles-based CM increased gradually with increasing sintering temperature from 6 nm (550 °C) to 180 nm (1100 °C), [21]. The preparation of CM derived from TiO_2 nano-particles without defect, has also been found to be more difficult than that of other membranes. In general, the separation layer is easy to crack as its thickness reduces, while incomplete and defective membranes can be formed if the coating layer is too thin. The thickness of the TiO_2 separation layer has been observed to increase linearly with the square root of dipping time in the range from 5 to 60 s. However, the thickness of the separation layer is often more than 50 times the diameter of the particles used for the active layer in order to coat continuously. In other words, micron-thick defect-free ceria film could be coated on microporous alumina support with high concentration of ceric sol (0.3-1 M) after the support was chemically treated firstly with acid and then with base.

1.2.8 Influence of concentration and pH on ceramic membranes

It is well known that pH and salt concentration have significant influence on CM performance. In order to manipulate such process and optimize its efficiency, it is very important to get insights into the effects of pH and salt concentration.

- **pH influence**

  The hydroxide titanium $-Ti-OH$ group present at the surface of CM varies in charge in function of pH. That happens according to reactions (7, 8) shown below as reported in [20].

$$-Ti-OH_{(s)} + H_3O^+ \xrightarrow{pH < 6} -Ti-OH_2^+(s) + H_2O \quad \{7\}$$

$$-Ti-OH_{(s)} + OH^- \xrightarrow{pH > 6} -Ti-O^-_{(s)} + H_2O \quad \{8\}$$

  Consequently the membrane charge varies with the pH. Then, the active layer of CM repels charged solute with equal electric charge. However, electro-neutrality is maintained with the adsorption of a counter-ion; onto the membrane. As a result, the permeability of the membrane to co-ions of salts and counter-ions vary.

  The salt rejection varies due to the mechanism previously explained. For example, as shown in figure 1.15, the membrane is positively charged at pH inferior to 6. So, positive co-ions Na^+, K^+ and Li^+ are repelled conversely to the counter-ion; Cl^- which is retained at membrane surface. The inverse analogy takes place at pH superior to 6, when the solution is alkaline. Furthermore, the Iso-Electric Point (IEP), is an intrinsic membrane characteristic that indicates when the membrane net charge is zero, and correspond to 0 rejection at pH 6, as shown in figure 1.15.

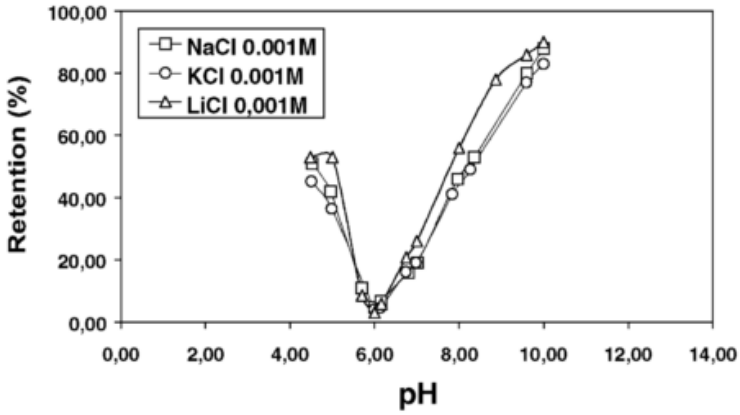

Figure 1.15: *pH influence on monovalent salt rejection, [20]*

- **Salt concentration influence**

The correlation between salt concentration, permeability and salt rejection in CM is described to be not obvious and sometimes confusing. Firstly, the concentration of dominant salt influence on rejection is shown in figure 1.16 and figure 1.17 for monovalent and divalent salts respectively.

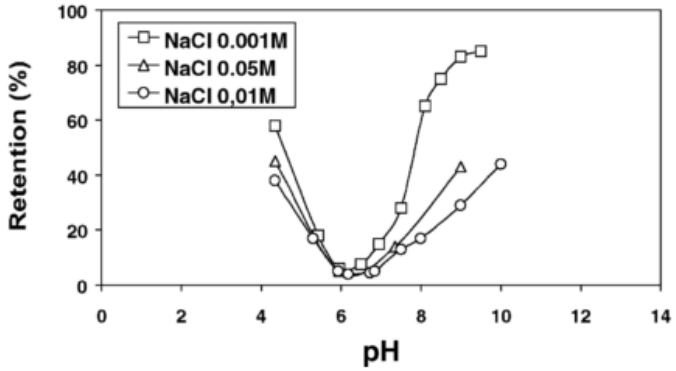

Figure 1.16: *Monovalent salt NaCl rejection, at different concentration, [20]*

The retention of NaCl is consistent with the change in pH and tend to be symmetric in acidic and alkaline conditions due to the equal number of counter-ions in both conditions. However, Na_2SO_4 retention tend to be greater in alkaline conditions due to sulphate electrostatic repulsion with the membrane negative charge.

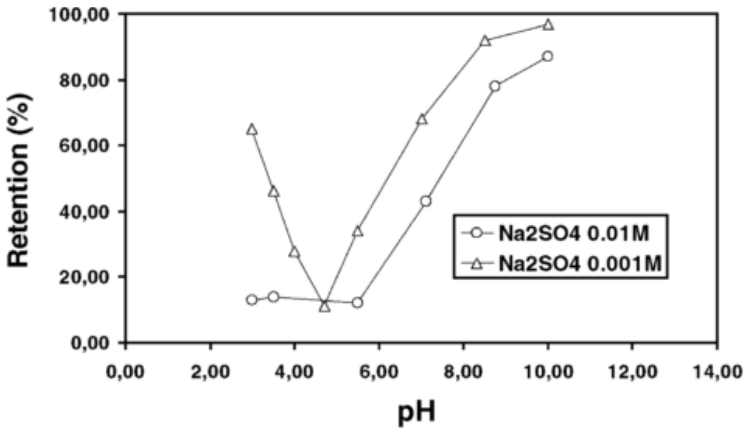

Figure 1.17: *Divalent salt Na_2SO_4 rejection, at different concentration, [20]*

Secondly, the salt-induced viscosity variation in membrane pore and bulk solution as stated in Bowen et al. [22], directly affects the membrane permeabilities to the attracted ions and then the salt rejection. As a the counter-ions enter are adsorbed into the membrane due to the electrostatic attraction, a large number of salt ions accumulate in/on the membrane pores forming an electric double layer, resulting in an increase of electro-viscous effect and thus increasing membrane permeabilities to these counter-ions. This can be observed in figure 1.17 where sulphate permeability increases and then the rejection decrease at 0.01 M because of sulphate screeming. Finally, as reported in Luo Jianquan et al. [23], higher salt concentration increases bulk viscosity, which decreases solute back-diffusion away from membrane, thus inducing more significant CPL and lower permeate flux. Generally, for a diluted solution, the permeate flux is mainly governed by solute rejection except at an extreme pH, while at a higher salt concentration, CPL becomes more significant. Figure 1.18 illustrates a general overview on pH and salt concentration influences on membrane properties.

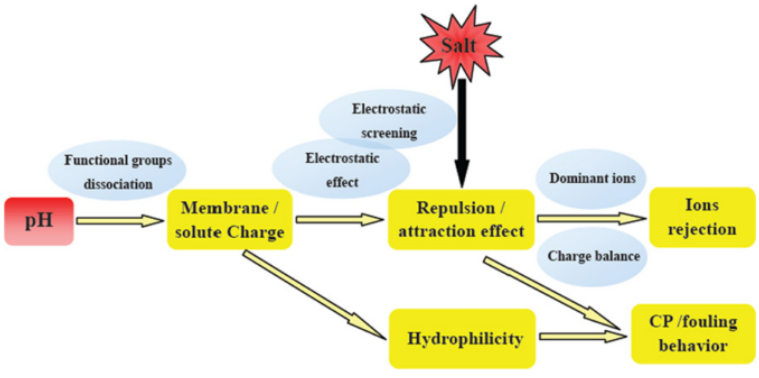

Figure 1.18: *Mechanism schematic of pH and salt effect: electrostatic interaction, [23]*

1.2.9 Comparison of NF ceramic and polymeric membranes and their application

Despite the fact, CM presents attractive features in various applications, polymeric membranes still dominate the market. The main reason for this situation is the over cost required to be afforded by the CM user. Often, CM cost three to five times as much as polymeric ones. As stated in [G. Vitaly et al,2016] [4], rough estimation on material cost evaluates 2000 $\$/m^2$ US dollar for ceramic membrane over 400 $\$/m^2$ for polymeric ones. Considering the higher fluxes and longer lifetimes of ceramic membranes, the difference becomes less dramatic, 60 $\$/m^2$ versus 20 $\$/m^2$ US dollar per unit of permeate volume, but still significant. The average 15 to 20 years lifespan of CM is roughly double than the 7 to 10 years of current polymeric membranes. In comparison to polymeric membranes, ceramic membranes are more resistant mechanically, thermally and chemically for example in acid/base recovery applications where the membrane can work under extreme pH range. Despite polymeric membranes are very flexible and yield good results for different conditions, they have a limitation to the long-term resistance and prove inadequate for application that requires high thermal and cleaning stability. To summarize, polymeric membranes are much cheaper than ceramic and are therefore preferred in new installations. However, CM require more expensive starting materials and their fabrication process is complex and consists of multiple stages. Moreover, their packing density in each module is low comparatively to polymeric ones. All that said, CM will gradually enter the industrial market and as expected their cost will be reduced for more application and use [4].

Chapter 2

OBJECTIVES

This project aims to extend the knowledge on AMD treatment using NF CM with a synthetic solution by studying the following aspects:

- The rejection of aluminium sulphate as dominant salt at different aluminium concentrations (300, 600 and 1900 ppm) at pH 1.

- The rejection of aluminium sulphate at pH 1 and 1.5 with aluminium Al^{3+} concentration at 600 ppm

- The effect of iron cation Fe^{3+} at 500 ppm on the rejection of aluminium sulphate as dominant salt at concentration 300 ppm and pH 1.

- The rejection of ferric sulphate as dominant salt at different iron concentrations (1000, 1500 and 2000 ppm) at pH 1.

- The influence of dominant salt, aluminium and ferric sulphate on the rejection of zinc, copper, calcium and rare earth element at pH 1.

- Calculate the membrane permeabilities to salt ions by modelling the experimental data to solution-film-diffusion-model (SDFM).

Chapter 3

EXPERIMENTAL METHODOLOGY

3.1 Lab-scale installation

In the introduction, AMD was described as low pH drainage with high concentration in sulphate salts. Also, solid-liquid filtration was introduced along with transport and exclusions mechanism as well as filtration technologies. Moreover, NF CM present interesting features for AMD treatment in order to reduce their negative impact. As observed in table 3.1, 7 synthetic solutions were elaborated and during the research 8 experiments were performed as the first solution was treated at pH 1 and 1.5. This section will outlines the experimental methodology, which can be broken down into lab-scale installation, analytical technique and data collection and modelling.

	Ions concentration (mg/l)						
	1	2	3	4	5	6	7
Aluminium	622.76 ± 3.99	1926.67 ± 7.43	373.68 ± 2.95	346.54 ± 0.84	344.79 ± 1.18	325.72 ± 1.44	302.53 ± 3.05
Calcium	24.27 ± 0.52	27.28 ± 0.01	27.28 ± 0.01	23.81 ± 0.25	26.12 ± 0.11	24.53 ± 0.16	23.49 ± 0.09
Copper	37.10 ± 0.21	34.66 ± 0.93	41.63 ± 0.39	43.56 ± 0.79	43.97 ± 1.09	38.9 ± 1.26	47.01 ± 2.63
Sulphate	1871.50 ± 16.99	6520.65 ± 153.80	2518.16 ± 30.12	2677.48 ± 31.98	3113.12 ± 55.77	3413.41 ± 42.08	3748.06 ± 39.21
Zinc	41.30 ± 0.44	45.92 ± 0.21	33.08 ± 0.31	38.08 ± 0.12	38.66 ± 0.43	39.06 ± 0.44	41.21 ± 0.86
Iron	-	-	-	455.89 ± 6.82	975.37 ± 17.41	1436.91 ± 17.05	1973.99 ± 27.88
Dysprosium	9.49 ± 0.04	8.28 ± 0.04	10.48 ± 0.08	10.15 ± 0.01	7.83 ± 0.07	8.25 ± 0.04	8.65 ± 0.05
Lathanum	8.8 ± 0.05	7.58 ± 0.12	9.14 ± 0.15	9.62 ± 0.02	7.08 ± 0.44	7.74 ± 0.03	8.14 ± 0.06
Neodymium	9.11 ± 0.04	8.06 ± 0.18	9.62 ± 0.14	9.39 ± 0.03	8.45 ± 2.10	8.64 ± 1.53	8.80 ± 1.04
Praseodymium	9.22 ± 0.01	7.99 ± 0.06	9.61 ± 0.09	10.02 ± 0.04	7.63 ± 0.21	8.04 ± 0.16	8.42 ± 0.13
Samarium	9.23 ± 0.04	7.97 ± 0.01	9.68 ± 0.01	7.01 ± 0.01	7.52 ± 0.13	7.88 ± 0.13	8.26 ± 0.14
Ytterbium	9.09 ± 0.04	7.72 ± 0.13	9.34 ± 0.17	9.83 ± 0.04	7.58 ± 0.07	7.95 ± 0.07	8.33 ± 0.09

Table 3.1: *Synthetic solutions with elements concentrations*

The tubular module used in this installation was a key component since it can be understood as a physical unit; that contains the membrane as shown in figure 3.2a. It is usually, made of stainless steel, as shown in figure 3.1b. Indeed, this material has very good properties to protect the installation against corrosion, as the experiment were performed in acidic conditions. This part of the installation has two main functions. Firstly, it provides an external enclosure to the CM, as illustrated in figure 3.2a, and protect it against over pressure up to 16 bar. Moreover, it collects the permeate, as shown in figure 3.2b to avoid leaking.

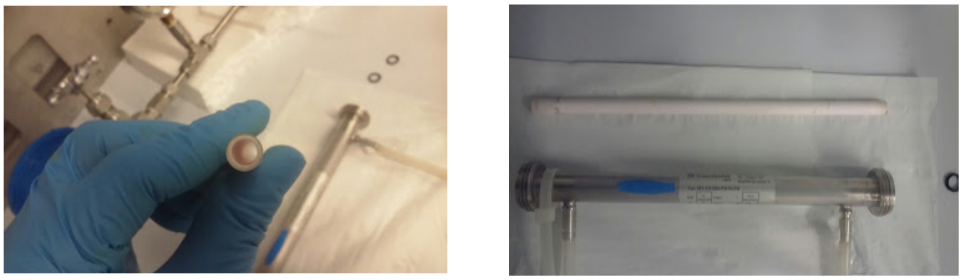

(a) *ceramic-membrane circular section* (b) *Ceramic-membrane and Fraunhofer module*

Figure 3.1: *Module and ceramic-membrane*

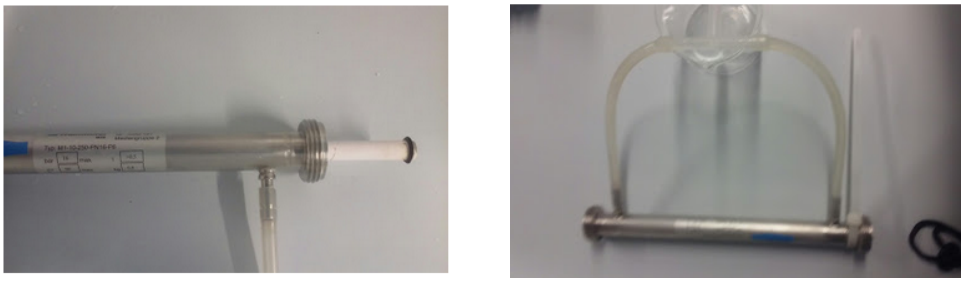

(a) *Ceramic-membrane inside the module* (b) *Module connections for permeate collection*

Figure 3.2: *Module as collector and membrane enclosure*

The membrane has an active layer made of titania TiO_2 which corresponds in the red rectangle of figure 3.3 to the smooth white surface a the top. Furthermore, it has a mean pore diameter of 1 nm, and it is supported on a Al_2O_3 solid phase, actually the gray granular surface, figure 3.3. As it has been mentioned, the configuration of the membrane was tubular with a circular section where the internal diameter was 6.5 mm. Furthermore, the thickness and the length were 2 mm and 220 mm, respectively and the membrane overall active area was 4493 mm^2.

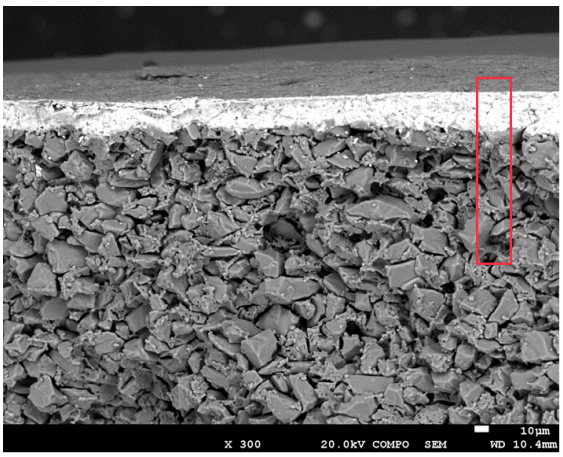

Figure 3.3: *SEM micrograph of TiO_2 membrane at 300x magnification, [24]*

In a previous study, the membrane was characterized to determine its IEP, by filtering 0.01 M Na_2SO_4 solutions from pH 1 to 11, [24]. The Na_2SO_4 rejections versus pH observed in that study are shown in figure 3.4. As observed, at lower pH values the membrane exhibited low rejections (20% aprox), due to the presence of positive charge of the TiO_2 membrane. Conversely, when the pH increased, the rejection also did as the membrane became negatively charged. The IEP was set at 5.5, since the membrane charges gradually changes with pH and increased in the rejection of Na_2SO_4.

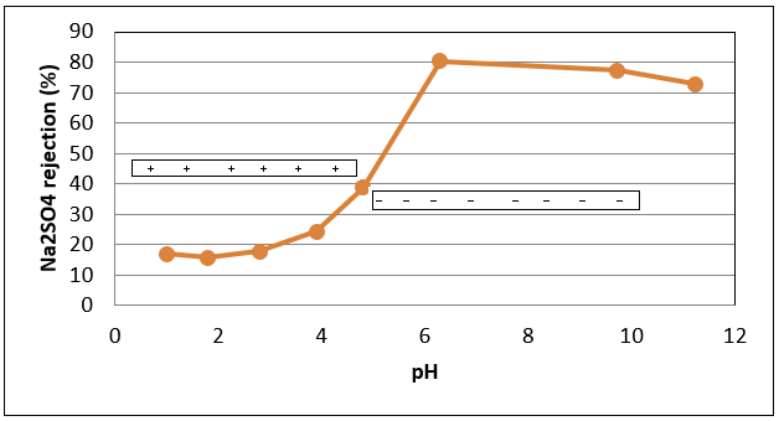

Figure 3.4: *0.01 M Na_2SO_4 rejection at 12 bar in pH range (1 to 11) for TiO_2 membrane, [24]*

During each experiment, the synthetic solution was stored in a 30 L, transparent PVC reservoir, stirred and refrigerated with a cooling system in order to maintain the temperature constant, figure 3.5a. Feed water was pumped to the membrane by means of a centrifuge pump figure 3.6a by acting on the by-pass valve, figure 3.5b. Also, a manometer was necessary to read the pressure before and after the module, figure 3.5b. A by-pass valve was used to increase and decrease the TMP and then, the solution-flow can be read in the flow-meter as shown in figure 3.5b.

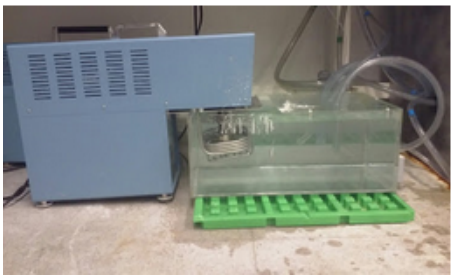

(a) *Tank and Thermostat for refrigeration*

(b) *Flow-meter (left), valves(center) and manometer (right)*

Figure 3.5: *Refrigeration system and basic instrumentation*

When crossing the module, the feed is divided in two streams: The permeate, which represents the fraction of the feed stream that have been passed through the CM, and the concentrate, which remains with the feed rising then the concentration of dissolved salt and

heavy metals. Both streams are recirculated to the tank; to maintain the initial conditions of the solution. Also, a pre-filter cartridge, figure 3.6b, helped to remove any macro-particle or debris from the concentrate before it was recirculated to the tank.

(a) *Motor pump* (b) *Pre-filter cartridge*

Figure 3.6: *Motor pump and pre-filter cartridge*

All these different equipments were combined together in a lab-scale plant to lead the investigation in NF. Figure 3.7 shows the process diagram where the different parts are integrated. Other instrumentation was assembled for experimental data collection such as TMP.

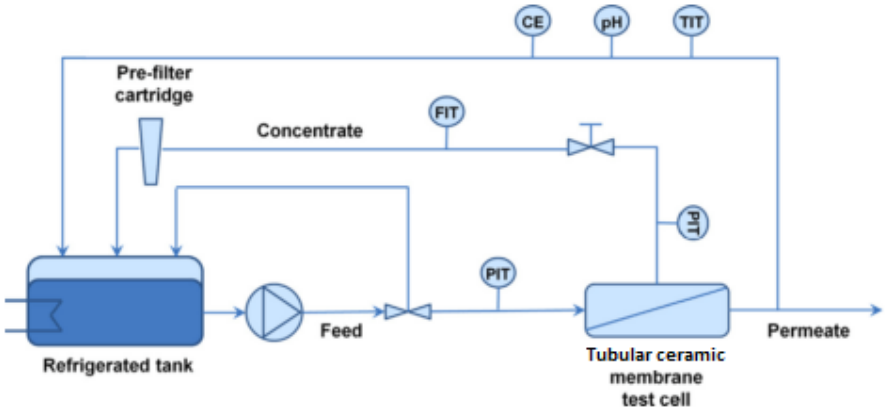

Figure 3.7: *Scheme of the Lab-scale NF plant*

3.1.1 Experimental operations

Each experiment can be separated in the following operations:

- **The pressurization of the membrane with water**

  Before the first use, CM was pressurised during 110 min, at 12 bar with pure water. For that, water supply, with pH and conductivity at 7.5 and 50.6 $\mu S \cdot cm^{-1}$ respectively, was used. The flow was maintained at 8 $L \cdot min^{-1}$ accordingly to the specifications. In

addition, the feed temperature was registered from the thermostat every 15 minutes, and then a sample was collected, followed by the measurement of pH and conductivity. After this stage the hydraulic permeability was calculated using equation (8). The value of this parameter was 9.11 $\mu m \cdot s^{-1} \cdot bar^{-1}$ and represents the lower limit for all cleaning task.

- **The pressurization of the membrane and experiment with the synthetic solution**

Each experiment began after the membrane pressurization with the synthetic solution for 110 min. As in the previous operation, the pressure was maintained at 12 bar and the flow rate at 8 $L \cdot min^{-1}$. This step aims to guaranty the same conditions overall the membrane's volume by making it "familiar" with the composition of the solution. Experiment run after solution pressurization, by varying inlet pressure from 5 to 12 bar with 15 min of dead time to stabilized the membrane at each scale. Also, a sample was collected for analysis during this period of time.

- **Membrane cleaning**

Inorganic fouling on the membrane might have occurred during the experiments. A cleaning protocol enabled to recover the membrane parameters such as flux and natural free-volume. At this stage, the hydraulic permeability K_w represents the key indicator of membrane quality after the operation. Two types of cleaning protocol and combination were implemented. Just after the experiment a cleaning operation was performed at 6 bar for 30 min and using only water as feed. However, this first wash was done few minutes after experimental session in order to prevent any no desired reaction between retained salts and the membrane components. Consecutively, other cleaning operation was performed using only water at 12 bar for 90 min. At the end, K_w was calculated and compared. The cleaning task ended if K_w was similar to the last value, with a difference < 10 %. Otherwise, another cleaning was executed for 30 min using 0.1 M H_2SO_4 solution at 9 bar before repeating another wash with water.

3.2 Sampling and analysis

3.2.1 Sampling

Firstly the feed and the permeate samples were periodically collected during the experiments and accurately labelled as shown in figure 3.8a. Secondly, the samples for metal, such as Fe, Al, Ca etc ; with sulphate salts and Rare Earth Element (REE) were filtered, adequately diluted when necessary and analysed by Induced Coupled Plasma Optical Emission Spectroscopy (ICP-OES),figure 3.8b. As result, the concentration of each solute were obtained using this technique. Specially, the concentration of sulphate was calculated by sulphur atomic detection. Also, the pH and the conductivity were useful to know during the preparation of the synthetic solution adding to the concentration measurement, in order to know some physico-chemical properties.

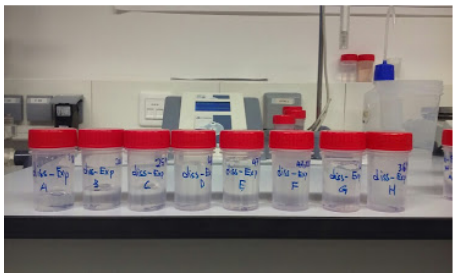

(a) *Feed and permeate sample identification*

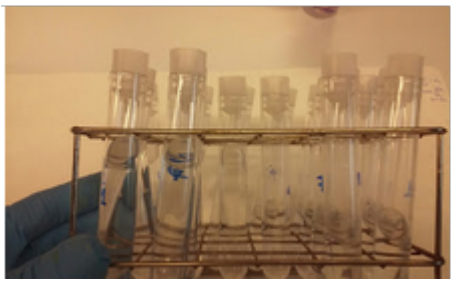

(b) *Diluted sample for ICP-OES analysis*

Figure 3.8: *Sample preparation*

3.2.2 Inductively coupled plasma

Inductively Coupled Plasma (ICP) is a valuable tool to analyse heavy metal and REEpresent in the samples. Generally, the instrument works by measuring a property which can be detected and then transformed into a signal. In the present case, Agilent Technology [5110 ICP-OES], figure 3.9, works by exciting each ion firstly and measuring their relaxation. A heat source up to 7000-8000 K and powered by pure argon, efficiently desolvates, vaporizes, excites and finally ionises atoms and molecules. The generated and excited ions emit a characteristic wavelength. Two modes of measurement are usually needed. The radial measurement is achieved with a radial detector, recommended for more concentrated samples, and axial measurement performed by the axial detector, useful for less concentrated samples, for the higher intensity in signal. ICP generally includes these different modules:

- Sample introduction system (nebulizer)
- cyclonic chamber, for bubble separation
- ICP torch, for heat generation
- High frequency generator
- Transfer optics and spectrometer, for measurement
- Computer interface, for data analysis and mapping

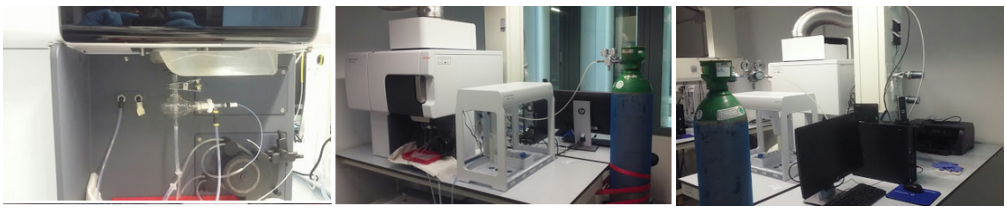

Figure 3.9: *Agilent Technology [5110 ICP-OES]*

3.2.3 Others instruments

- **Conductivity-meter**
  Electric conductivity represents the ability to flow electric current in a material, and is closely related to the present of charged particles. So, the conductivity-meter measures the solution conductance by applying an electric current. Consequently, an increase in the average of dissolved ions means more conductance. The apparatus (Sension EC7 Basic) is shown in figure 3.10.

Figure 3.10: *Conductivity-meter, Sension EC7 Basic*

- **pH-meter**
  The pH indicates the concentration of proton present in a solution. However, it was measured using the apparatus (Crison GLP 21) shown in figure 3.11.

Figure 3.11: *pH-meter, Crison GLP 21*

3.3 Data collection and mathematical modelling

The collection of data is an important task in any method for the process evaluation and analysis. In this project some data were acquired with the instruments previously mentioned. Consecutively, they were verified and were used for others variable calculation, listed below.

- **Measured variables**
  - **Feed pH**: measured with the pH meter.
  - **Permeate pH**: measured with the pH meter.
  - **Pressure IN** [P_{in}]: measured with a manometer (bar).
  - **Pressure OUT** [P_{out}]: measured with a manometer (bar).
  - **Feed conductivity** [C_f]: measured with the conductivity meter ($mS \cdot cm^{-1}$).
  - **Permeate conductivity** [C_p]: measured with the conductivity meter ($mS \cdot cm^{-1}$).

- **Feed Temperature** [T_f]: measured with the tank thermostat (°C).
- **Permeate Temperature** [T_p]: measured with the conductivity meter (°C).
- **Sampling time** [T_s]: measured with a chronometer (min)

- **Calculated variables**
  - **Trans-membrane pressure** [TMP]: is calculated with

$$TMP = \frac{P_{in} + P_{out}}{2} \tag{3.1}$$

    where:
    TMP is the pressure crossing the module or the membrane [bar].
  - **trans-membrane flux** [J_v: $\mu \cdot m \cdot s^{-1}$]: is calculated with

$$J_v = \frac{m_s}{t_p \cdot \rho \cdot A \cdot 10^{6}} \tag{3.2}$$

    where:
    A is the area of the membrane [m^2]
    t_p is the sampling time [s]
    ρ is the solution density [$Kg \cdot m^{-3}$]
    m_s is the permeate mass [kg]
  - **Hydraulic permeability** [K_w: $\mu m \cdot s^{-1} \cdot bar^{-1}$]: is calculated with

$$K_w = \frac{J_v}{TMP} \tag{3.3}$$

  - **Observable rejection** [$R_o$bs]: is calculated with

$$R_{obs} = (\frac{C_f - C_p}{C_f}) \cdot 100 \tag{3.4}$$

    where:
    C_f is a solute concentration in the feed [$mol \cdot l^{-1}$]
    C_p is a solute concentration in the permeate [$mol \cdot l^{-1}$]

3.3.1 Solution-diffusion-film-model

The Solution-Diffusion-Film-Model (SDFM) is a mathematical model used in non-porous membranes, specially in NF to characterize and predict the interactions between a membrane and an electrolytic solution containing a dominant salt with higher concentration than others trace salts present. Generally, the model works by considering that the transport of solute mainly depends on solute diffusion through the membrane and electric migration, [8].

Firstly, the observable rejection ${R_s}^{Obs}$ of the dominant salt is calculated using equation (3.4). After that, the obtained values are adjusted by equation equation (3.5).

$$R_s^{obs} \equiv 1 - \frac{c_s''}{c_s'} = \frac{\frac{J_v}{P_s}\exp\left(-\frac{J_v}{P_s^{(\delta)}}\right)}{1+\frac{J_v}{P_s}\exp\left(-\frac{J_v}{P_s^{(\delta)}}\right)} \tag{3.5}$$

Where

$C_s{}^{'}$ and $C_s{}^{''}$ are the concentration of dominant salt in feed and permeate respectively.

Consecutively to the adjustment of dominant salt permeability P_s and CPL permeability $P_s{}^{\delta}$, the concentration of solute at the surface of the membrane $C_s{}^{m}$ can be estimated using equation (3.6). Also, $R_s{}^{\mathrm{Int}}$ is calculated as solute rejection between permeate and membrane surface.

$$R_s^{int} \equiv 1 - \frac{c_s''}{c_s^{(m)}} = \frac{\frac{J_v}{P_s}}{1+\frac{J_v}{P_s}} \tag{3.6}$$

The concentration of trace ion at the membrane surface $C_t{}^{m}$ and thus, the $R_t{}^{\mathrm{Int}}$ is also calculated using equation (3.7), with the estimated value of CPL thickness δ and diffusion coefficients of ions $D_{+/-,s}{}^{\delta}$.

$$\frac{c_t^{(m)}}{c_t'} = \exp(Pe_t)\left[1+R_s^{obs}(exp(Pe_s)-1)\right]^{b^{(\delta)}} \times\left\{1-\left(1-R_t^{obs}\right)\int_{\exp(-Pe_t)}^{1}\frac{dy}{\left[1+R_s^{obs}(y^{-\alpha}-1)\right]^{b^{(\delta)}}}\right\} \tag{3.7}$$

Where:
$C_t{}^{'}$ is the concentration of trace ion in the feed, $[\mathrm{mol}\cdot\mathrm{m}^{-3}]$.
$C_t{}^{''}$ is the concentration of trace ion in the permeate, $[\mathrm{mol}\cdot\mathrm{m}^{-3}]$.
$D_s{}^{\delta}$ is the diffusion coefficient of dominant salt in CPL, $[\mathrm{m}^2\cdot\mathrm{s}^{-1}]$.
$Z_{+/-}$ is the charge of a single ion of dominant salt, $[+/-]$.
Pe_s is the Peclet number of dominant salt.
Pe_t is the Peclet number of trace ion.
$D_t{}^{\delta}$ is the diffusion coefficient of trace ion in the CPL, $[\mathrm{m}^2\cdot\mathrm{s}^{-1}]$.
Z_t is the charge of trace ion the CPL, $[+/-]$.

The dominant salt concentration gradient inside the CPL, creates an electric field from

the difference between diffusions coefficients. The field in turn, interacts with ions. When there is a single dominant salt and trace ions, the reciprocal intrinsic trans-membrane passage of a trace ion f_t can be represented as a function of reciprocal intrinsic trans-membrane passage of dominant salt f_s, equation (3.8).

$$f_t = (f_s)^b + K\left(\frac{f_s - (f_s)^b}{1-b}\right) \tag{3.8}$$

Finally, the membrane permeabilities to single ions of dominant salt $P_{+/-}$ are estimated using equation (3.9) and the membrane permeability to trace ion P_t are also estimated using equation (3.10).

$$P_{\pm} = \frac{P_s}{1-\left(\frac{Z_{\pm}}{Z_t}\right)b} \tag{3.9}$$

$$P_t \equiv \frac{P_s}{K} \tag{3.10}$$

Others parameters of the model are summarized in table 3.2.

$Pe_{s,t} = J_v \,{}^{\delta}\!/_{D^{\delta}_{s,t}}$	Is the Peclet number of dominant salt or trace ion
$D_s^{\delta} = \frac{(Z_+ - Z_-)D_+D_-}{Z_+D_+ - Z_-D_-}$	Is the diffusion coefficient of the dominant salt in the unstirred layer
$b^{(\delta)} = \frac{Z_t(D_+ - D_-)}{Z_+D_+ - Z_-D_-}$	Is the dimensionless diffusion coefficient
$\alpha = {D_t^{\delta}}/{D_s^{\delta}}$	Is the ratio of the diffusion coefficient of the trace ion respect to the dominant salt
$f_{s,t} = \frac{c_{s,t}^{(m)}}{c_{s,t}''} = \frac{1}{1-R_{s,t}}$	Is the passage of dominant salt or trace ion
$\delta = \frac{D_s^{(\delta)}}{P_s^{(\delta)}}$	Is the concentration-polarization layer thickness

Table 3.2: *Variables and parameters of SDFM, [6]*

Chapter 4

RESULTS AND ANALYSIS

4.1 Solute rejection and membrane permeabilities to dominant salts

The impacts of pH and salt concentration on NF are mainly reflected in the variation of flux, solute rejection and the permeability of the membrane. However, the solute rejection and fouling also depend on both solute type and the composition of the solution. After performing several experiments with CM, the experimental data were used in order to calculate the solutes rejections and consecutively they were fitted by the SDFM model, introduced in the experimental methodology, in order to calculate the membrane permeabilities to the different ions of study. The results extend on different salts, mainly at different concentration of $Al_2(SO_4)_3$ and $Fe_2(SO_4)_3$ with others traces ions, in special REE as listed in table 3.1. Figure 4.1 shows the data treatment process with different optimizations whose results will be the main discussion in this section. Finally, the speciation diagrams are regularly introduced to highlight the species present at different pH and related them with the membrane behaviour.

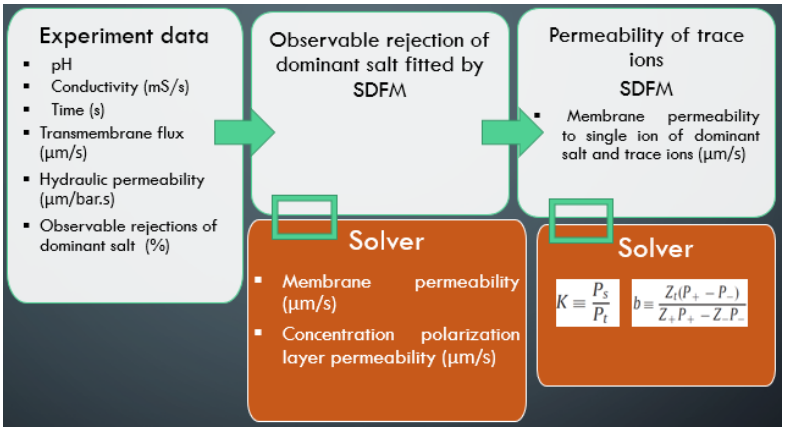

Figure 4.1: *Data treatment diagram process*

As mentioned before, membrane and CPL permeabilities to dominant salt set out dominant ions permeabilitiies for the CM. The values obtained for dominant salts, $Al_2(SO_4)_3$

and $Fe_2(SO_4)_3$ are listed in table 4.1. They showed a variation in the behaviour of both membrane and CPL for different type of dominant ions of the dominant salt, the pH and the concentrations of dominant ions.

		Permeability [µm.s-1]		
Dominant salt	Concentration [ppm]	Membrane	Concentration Polarization Layer	pH
$Al_2(SO_4)_3$	Al: 300	70.78	72.14	1.00
	Al: 600	95.48	79.95	1.50
	Al: 600	144.30	113.19	1.00
	Al: 1926	98.14	82.65	1.00
	Fe: 500 ; Al: 300	39.78	53.00	1.00
$Fe_2(SO_4)_3$	Fe: 1000	81.13	88.44	1.00
	Fe: 1500	40.95	56.12	1.00
	Fe: 2000	30.17	52.50	1.00

Table 4.1: *Membrane and CPL permeabilities to dominant salt, calculated for each experiment*

4.1.1 The impact of aluminium concentration on the removal of dominant salt, $Al_2(SO_4)_3$

At constant TMP, the solvent permeation flux and solute rejection mainly depend on three factors, the concentration difference between feed and permeate, CPL resistance and finally the membrane permeability. The variations of these factors are completely controlled by the exclusions and transport mechanisms stated previously. For example, for $Al_2(SO_4)_3$ as dominant salt, its dissociation leads to the apparition of various species which individually interact with the membrane. Indeed, the complexes formed during the speciation of the dominant salt vary with the cations charges, concentration, and finally the pH the solution. Figure 4.2 shows the speciation diagram for $Al_2(SO_4)_3$ at 600 ppm indicating the presence of the following species $Al(SO_4)^+$, $Al(SO_4)_2{}^-$, $H(SO_4)^-$ and $SO_4{}^{2-}$.

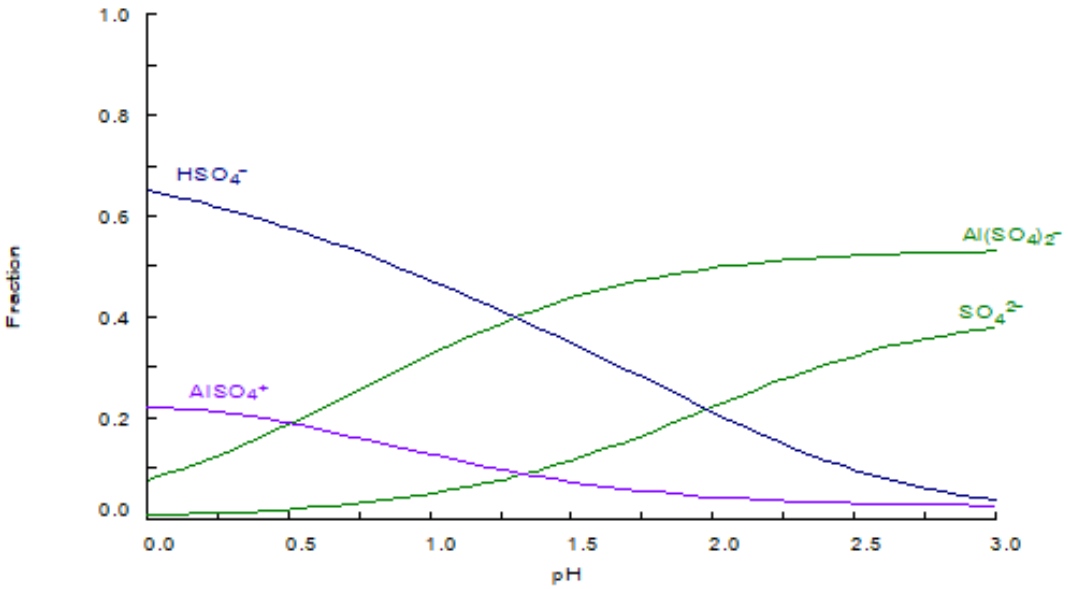

Figure 4.2: *$Al_2(SO_4)_3$ speciation diagram at 600 ppm of aluminium*

It is widely known that DE and DiE are important exclusions mechanisms in NF and that the TiO_2 membrane used in this project is expected to be positively charged in acidic conditions. However, DE limits the cations passage and thus their rejection which is high. So, $Al(SO_4)_2^-$, $H(SO_4)^-$ and SO_4^{2-} are expected to be less rejected than $Al(SO_4)^+$, because of the presence of electrostatic attraction and repulsion forces between the charges of the membrane and the species. Moreover, any ionic species passage can be described using DiE whose contribution is an electrostatic force proportional to the charge of the ion and depends on the interaction with the solvent. So, water in this case, by DiE will decrease SO_4^{2-} permeance than the others species. As a result, the expected individual rejection sequence under these conditions, is the following $R(Al(SO_4)^+)>R(SO_4^{2-})>R(Al(SO_4)_2^-)>R(HSO_4^-)$. Consequently the CPL appears to have a notable concentration in SO_4^{2-}. For the experiment with 600 ppm of aluminium at pH 1, the ionic membrane permeability to sulphate and aluminium, as listed in table 4.3 are 180.38 $\mu m \cdot s^{-1}$ and 111.00 $\mu m \cdot s^{-1}$ respectively. This observation indicates that sulphate is less rejected than aluminium in the CM. However at pH 1.5 aluminium sulphate $Al_2(SO_4)_3$ presents lower membrane and CPL permeabilities as shown in table 4.1 for the same experiment, 144.30 $\mu m \cdot s^{-1}$ and 113.19 $\mu m \cdot s^{-1}$ respectively.

The variation of aluminium and sulphate concentrations also have influences on the synthetic solution and the membrane properties. Although, the species present in the solution are the same, their fractions vary as shown in figure 4.3. $Al(SO_4)^+$ is so far the dominant species at pH 1 and 300 ppm of aluminium (figure 4.3). At 1800 ppm the increment of aluminium leads to a moderate distribution between $Al(SO_4)^+$ and $Al(SO_4)_2^-$, where the latter is the dominant specie, (figure 4.4).

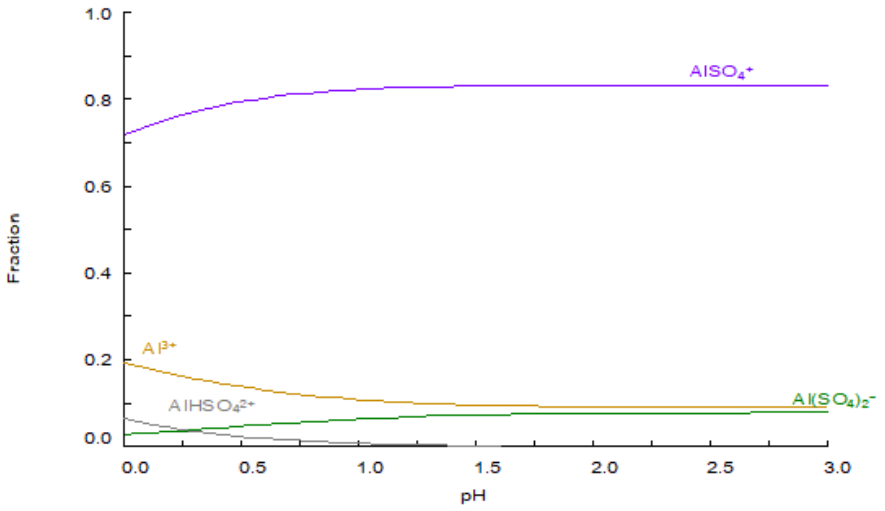

Figure 4.3: *$Al_2(SO_4)_3$ speciation diagram, 300 ppm of aluminium*

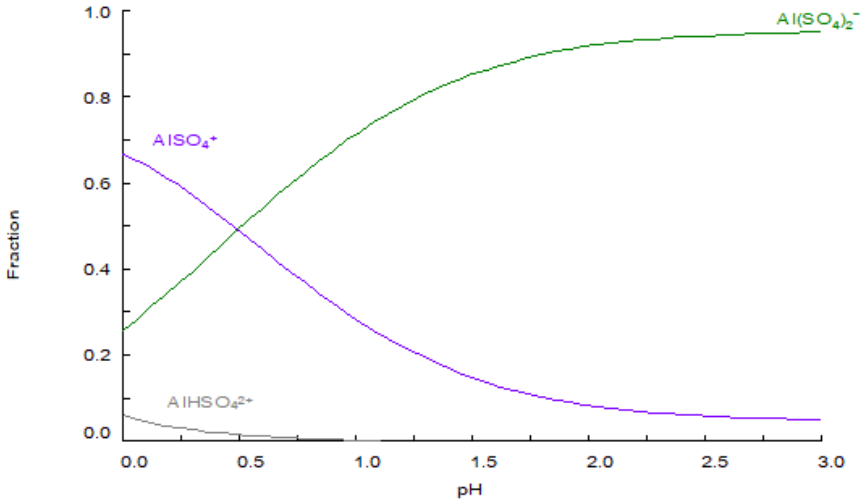

Figure 4.4: *$Al_2(SO_4)_3$ speciation diagram, 1900 ppm of aluminium*

Due to that, the analysis of membrane permeabilities to ions and dominant salt set out important variations and evidences. Firstly, the values of the membrane permeabilities to the ions of study , listed in table 4.2 indicates that the increase of aluminium concentration rises Al^{3+} and $Al(SO_4)_2^-$ individual permeabilities. As observed, the total values for each ions were 163.06, 180.38 and 196.28 $\mu m \cdot s^{-1}$ for sulphate and 38.31, 111.00 and 56.08 $\mu m \cdot s^{-1}$ for aluminium respectively at 300, 600 and 1800 ppm. It is clear that the membrane tends to reject more aluminium than sulphate and when the amount of available sulphate ions is not balanced with aluminium, the permeability of this latter increase which consequently decrease the solute rejection.

		Membrane permeance to each ion [µm·s-1]								
		Al_300_pH_1			Al_600_pH_1			Al_1800_pH_1		
		[Al +3]	[SO4 -2]	[Ions]	[Al +3]	[SO4 -2]	[Ions]	[Al +3]	[SO4 -2]	[Ions]
Bivalent [+2]	Zinc	38.31	163.06	74.50	111.00	180.38	277.98	56.08	196.28	137.66
	Calcium			88.40			710.53			848.43
	Copper			81.95			321.98			132.53
Trivalent [+3]	Lanthanum			45.60			128.98			82.40
	Praseodymium			46.86			132.16			84.31
	Neodymium			45.92			131.76			83.16
	Samarium			45.98			131.17			83.32
	Ytterbium			38.82			111.88			72.74
	Dysprosium			43.64			122.89			79.31

Table 4.2: *Dominant salts and trace ions permeance, alumnium sulphate (300,600,1800 ppm), pH 1*

For example, aluminium permeabilities rises from 38.31 to 111.00 $\mu m \cdot s^{-1}$, when sulphate concentrations were 2518 and 1871 ppm respectively. That can be explained using the individual interactions of $Al(SO_4)_2^-$ and HSO_4^- with the CM. As they hold a single negative charge, the influence of DE attracted them to the membrane. However, in contrast, the effect of DiE on them is very weak. As result, they are more active crossing the membrane. Nevertheless, the activity of HSO_4^- is more significant, as the presence of protons enable it to gain additional

mobility for its higher diffusion coefficient. All that said, there is not a clear pattern in both membrane and CPL permeabilities to dominant salt as shown in table 4.1. However, a great difference between membrane and CPL permeability can indicate a poor performance. Finally, the observable rejection of $Al_2(SO_4)_3$, at different concentrations of aluminium and sulphate fitted by SDFM are shown in figure 4.5.

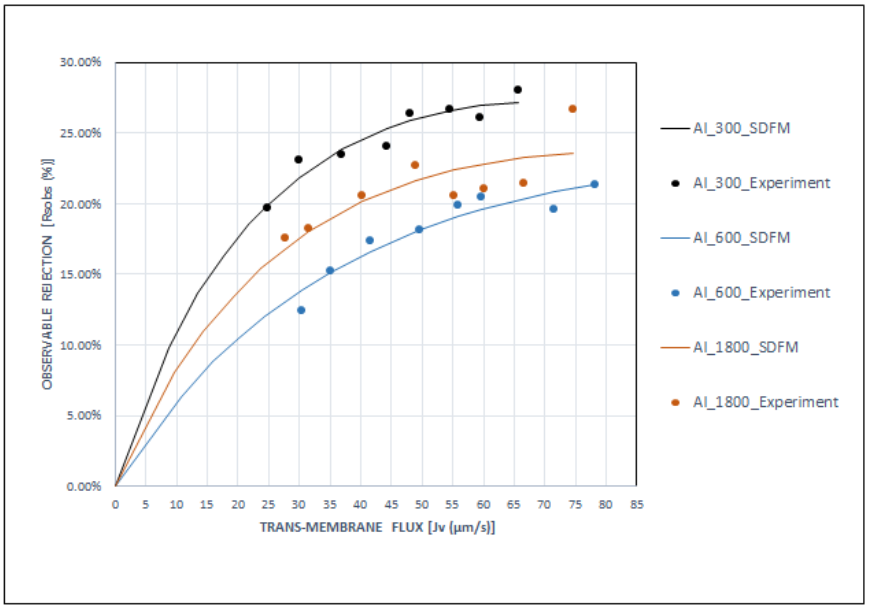

Figure 4.5: *Dominant salt, $Al_2(SO_4)_3$ rejection, at different concentration [(dot)experimental point,(line)model prediction]*

4.1.2 The impact of the pH solution on the removal of dominant salt, $Al_2(SO_4)_3$

In this study case the influence of pH on CM was evaluated with the solution feed at pH 1 and 1.5 on one hand, and on the other maintaining sulphate aluminium, as dominant salt with the concentration of aluminium at 600 ppm. In analogy to what has been said before, an useful information to know firstly is the speciation of $Al_2(SO_4)_3$ at pH 1.5. A backwards view to figure 4.2 indicates the following sequence for the distribution of species is, $R(Al(SO_4)_2^-)>R(HSO_4^-)>>R(SO_4^{2-})>R(Al(SO_4)^+)$. As stated, $Al(SO_4)_2^-$ and HSO_4^- rejections are lower comparatively to $Al(SO_4)^+$ and SO_4^{2-}. The reason is their attraction to the membrane by DE and the weak impact of DiE. As shown in figure 4.6, the maximum solute rejections were quite similar (20% and 23%) as well as water flux, nearly 80 $\mu m \cdot s^{-1}$ in both cases. Adding to that, the permeance of the membrane to each ions are outlined in 4.3; and indicates that decreasing the pH from 1.5 to 1, the membrane permeance of SO_4^{2-} increased from 129.03 to 180.38 $\mu m \cdot s^{-1}$. A backward view to figure 4.2 indicates that at pH 1; the fraction of HSO_4^- increases while it decreases for SO_4^{2-}; because of the equilibrium between H^+ and SO_4^{2-} at pK 1.92. So, the composition of SO_4^{2-} is lower in comparison with HSO_4^- which is easily transported due to DiE. With these findings, it would be wise to consider that the global influence of pH on dominant salt rejection require more accurate studies. Simply because the pH difference is too small to appreciate any remarkable changes. So, there are good reasons

to conduct more studies in order to understand how pH variation can influence the interaction between a dominant salt, such as $Al_2(SO_4)_3$ or $Fe_2(SO_4)_3$ and CM.

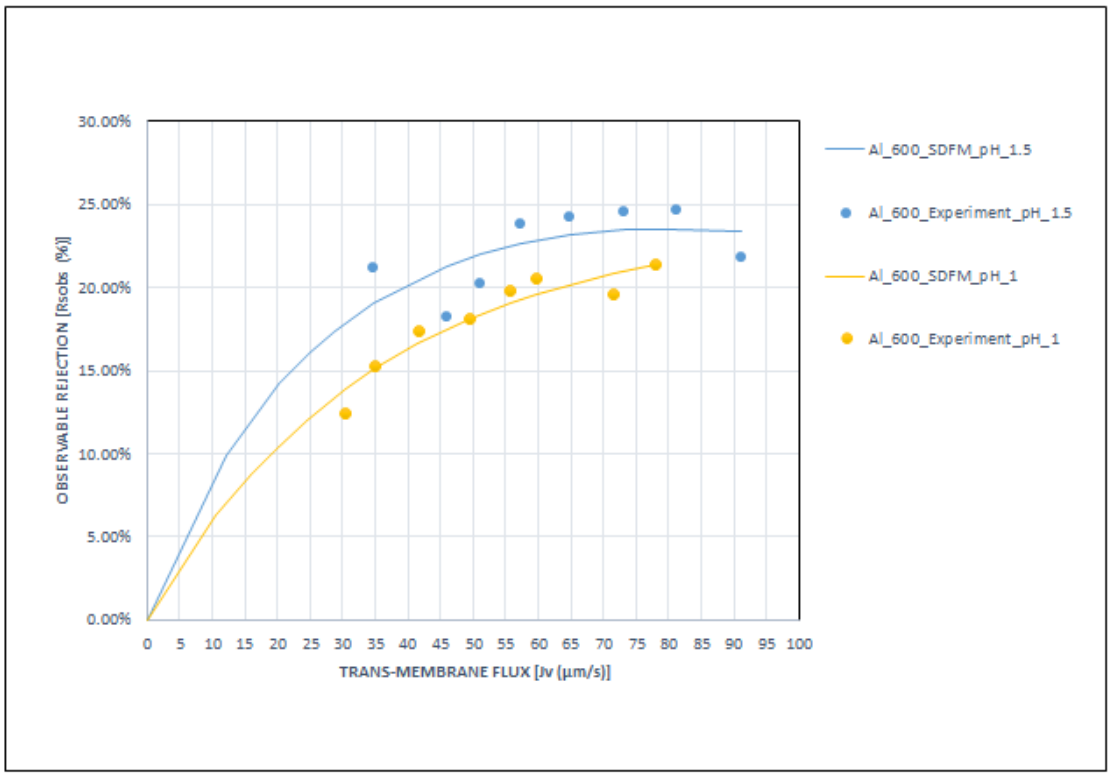

Figure 4.6: *Dominant salt, $Al_2(SO_4)_3$ rejection, at pH 1 and 1.5 [(dot) experimental point,(line) model]*

		Membrane permeance to each ion [µm·s-1]					
		Al_600_pH_1.5			Al_600_pH_1		
		[Al +3]	[SO4 -2]	[Ions]	[Al +3]	[SO4 -2]	[Ions]
Bivalent [+2]	Zinc	68.98	129.03	179.07	111.00	180.38	277.98
	Calcium			201.85			710.53
	Copper			166.30			321.98
Trivalent [+3]	Lanthanum			112.92			128.98
	Praseodymium			115.38			132.16
	Neodymium			113.20			131.76
	Samarium			114.12			131.17
	Ytterbium			94.45			111.88
	Dysprosium			106.83			122.89

Table 4.3: *Dominant salt and traces ions permeance, aluminium concentration (640 ppm) at pH 1 and 1.5*

4.1.3 The impact of Fe^{3+} on the removal of dominant salt, $Al_2(SO_4)_3$

$Al_2(SO_4)_3$ was maintained as dominant salt with 300 ppm of aluminium, however 500 ppm of iron(III) was added to study its influence on $Al_2(SO_4)_3$ rejection and permeate flux. At first sight, there is a clear difference with the experiments performed using only aluminium. As observed in figure 4.7, $Al_2(SO_4)_3$ rejection increase from nearly 27% to 35%; maintaining the maximum flux at 65 $\mu m \cdot s^{-1}$ approximately.

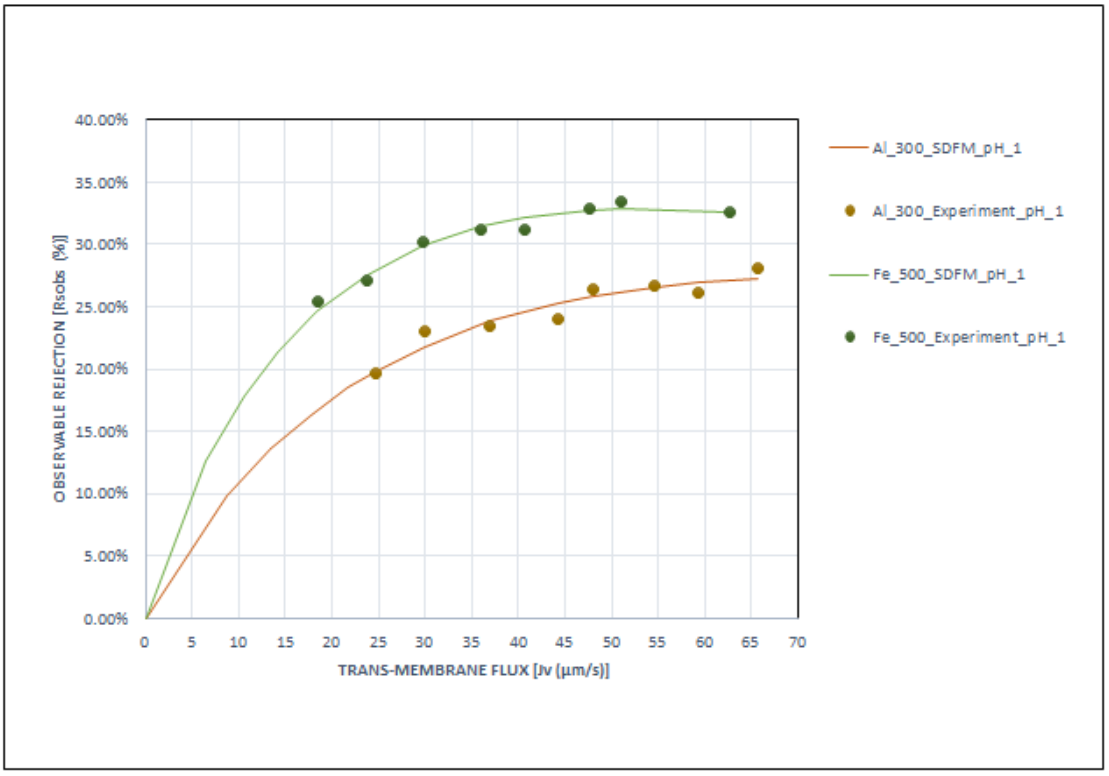

Figure 4.7: *Dominant salt, $Al_2(SO_4)_3$ rejection for solutions with and without Fe^{3+}, [(dot) experimental point,(line) model]*

Despite these results were unexpected, their correlation with the interactions of ionic species can be a start point to characterize this performance. New ionic species can be identified in figure 4.8 in addition to the ionic species listed previously in the presence of aluminium. For instance, $FeHSO_4^{2+}$, $FeSO_4^{+}$ and $Fe(SO_4)_2^{-}$ are new species which passage can be described with DE and DiE. Similarly to previous statements, all the species are attracted or repelled depending on their charges by DE. So $FeHSO_4^{2+}$ and $FeSO_4^{+}$ are repelled and $Fe(SO_4)_2^{-}$ is attracted to the membrane active layer. However, the passage of $Fe(SO_4)_2^{-}$ is enhance by water molecules decreasing sightly his individual rejection. As result, the individual rejection sequence of these species is the following, $R(FeHSO_4^{2+}) >> R(FeSO_4^{+}) > R(Fe(SO_4)_2^{-})$. So, the contribution of these individual rejection clearly improves $Al_2(SO_4)_3$ rejection as dominant salt.

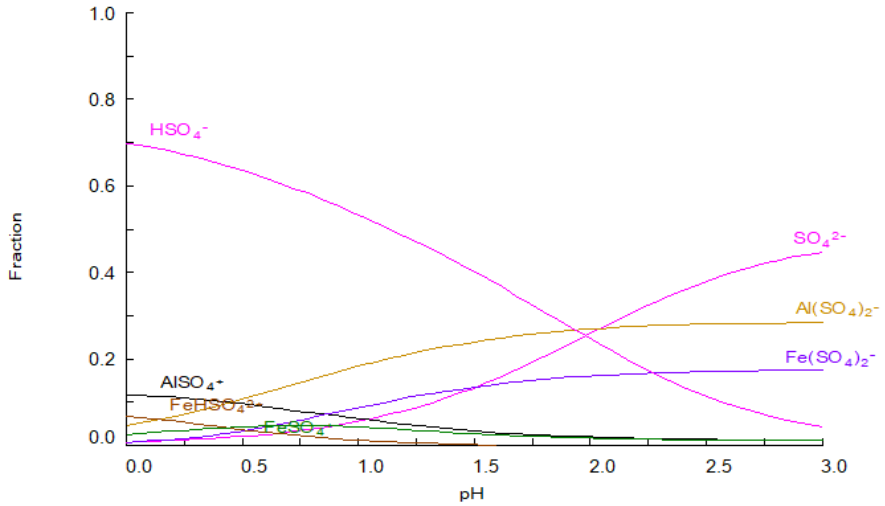

Figure 4.8: *Sulphate speciation diagram,(Al^{3+}-300 ppm) (Fe^{3+}-500 ppm)*

The results of the membrane permeability to the ions of study are presented in table 4.4. As observed, the membrane permeabilities to aluminium remains constant at nearly 39.00 $\mu m \cdot s^{-1}$. In contrast, sulphate permeance drastically decrease from 163.06 to 39.78 $\mu m \cdot s^{-1}$ due to the presence of ferric ions which extend the number of available complexes for sulphate speciation.

		Membrane permeance to each ion [µm·s-1]					
		Fe_500_pH_1			Al_300_pH_1		
		[Al +3]	[SO4 -2]	[Ions]	[Al +3]	[SO4 -2]	[Ions]
Bivalent [+2]	Zinc	39.77	39.78	90.70	38.31	163.06	74.50
	Calcium			123.12			88.40
	Copper			102.86			81.95
Trivalent [+3]	Lanthanum			63.28			45.60
	Praseodymium			64.79			46.86
	Neodymium			62.54			45.92
	Samarium			60.09			45.98
	Ytterbium			44.53			38.82
	Dysprosium			44.53			43.64

Table 4.4: *Dominant salt and traces ions permeance, aluminium(300 ppm) - iron(500 ppm)*

4.1.4 The impact of iron Fe^{3+} concentration on the removal of dominant salt, $Fe_2(SO_4)_3$

As outlined in the introduction, iron is a key component during AMD formation because of its important proportion in sulphite mineral. Consequently, ferric species have relevant concentrations in AMD samples. This evidence gives strength to study CM performance with $Fe_2(SO_4)_3$ solutions. As mentioned when aluminium sulphate was dominant salt, the overall solute rejection relies on the exclusion of the ionic species present in the solution. Thus, the

speciation of $Fe_2(SO_4)_3$ is shown in figure 4.9. Firstly, iron concentration does not have a remarkable impact on speciation, consequently as depicted in figure 4.9a and 4.9b both diagrams look similar in complex species fractions. However, three different complexes can be identified in both figures $FeHSO_4{}^{2+}$, $FeSO_4{}^{+}$ and $Fe(SO_4)_2{}^{-}$. Adding to that, the same exclusions mechanism mentioned in previous sections rule their migration through the CM. Seemingly to the solutions with aluminium, CM behaves equally with ferric species in these experimental conditions. Consequently, the individual rejection sequence is the following, $R(FeHSO_4{}^{2+}) >> R(FeSO_4{}^{+}) > R(Fe(SO_4)_2{}^{-})$.

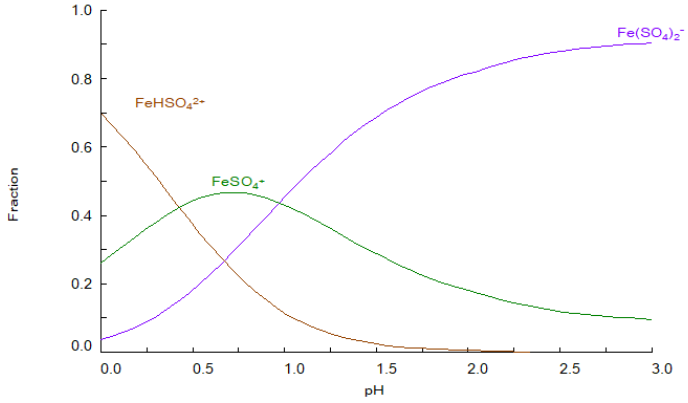

(a) *$Fe_2(SO_4)_3$ speciation diagram, 1000 ppm of iron*

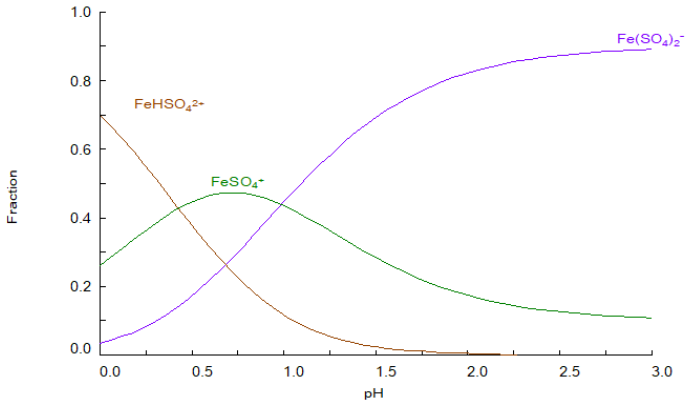

(b) *$Fe_2(SO_4)_3$ speciation diagram, 2000 ppm of iron*

Figure 4.9: *$Fe_2(SO_4)_3$ speciation diagrams at different concentrations*

The results of solute rejection calculated and fitted by SDFM as shown in figure 4.10 entail an important fact comparatively to $Al_2(SO_4)_3$ as dominant salt. The dominant salt rejection increases with the amount of iron(III), as shown in figure 4.10, the maximum rejections were 30%, 35% and 40 % at 1000, 1500 and 2000 ppm of iron Fe^{3+} respectively. That can be mainly attributed to the contribution of CPL intensification, where the permeabilities as listed in table 4.1, decrease from 88.44 to 52.50 $\mu m \cdot s^{-1}$ which consequently leads to a considerable reduction of permeate flux from 85 to 45 $\mu m \cdot s^{-1}$, as depicted in figure 4.10.

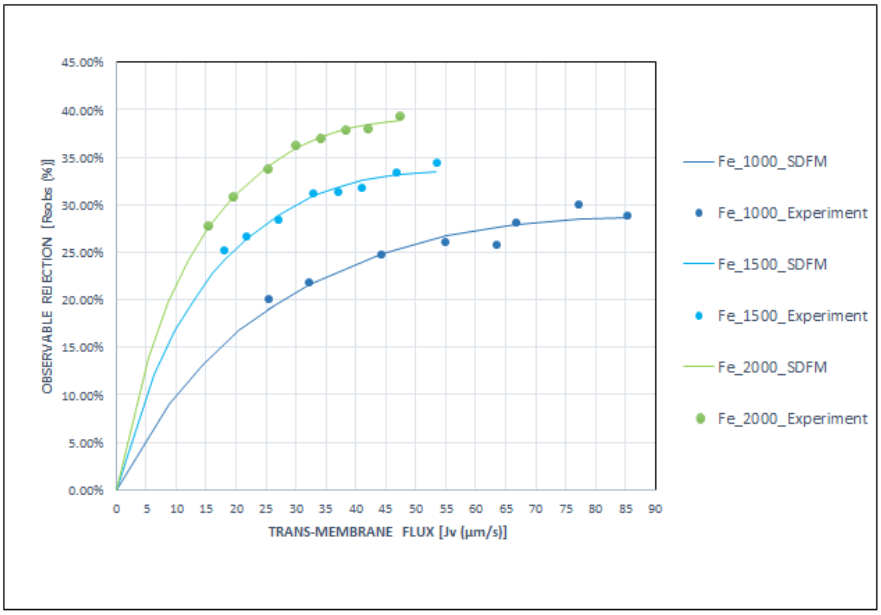

Figure 4.10: *Dominant salt, $Fe_2(SO_4)_3$ rejection at different concentration [(dot)experimental point,(line) model]*

Finally the membrane permeance to each ions are resumed in table 4.5 and 4.6. In the view of these outcomes, it is clear that the CM presents an important resistance to ferric cation. For example, the comparison of permeabilities in table 4.6 lists 56.08 $\mu m \cdot s^{-1}$ for aluminium and 17.24 $\mu m \cdot s^{-1}$ for iron(III). Also, the transport trough the TiO_2 membrane was easier for aluminium than iron. However, this aspect is not a main subject within this study.

		Membrane permeance to each ion [µm·s-1]					
		Fe_1000_pH_1			Fe_1500_pH_1		
		[Fe +3]	[SO4 -2]	[Ions]	[Fe +3]	[SO4 -2]	[Ions]
Bivalent [+2]	Zinc	70.55	90.14	77.62	23.40	81.90	31.45
	Calcium			59.42			44.45
	Copper			102.05			36.47
Trivalent [+3]	Lanthanum			58.33			26.05
	Praseodymium			52.74			26.20
	Neodymium			50.65			25.52
	Samarium			51.38			26.03
	Ytterbium			39.90			21.02
	Dysprosium			50.81			24.98

Table 4.5: *Dominant salts and trace ions permeance, Fe^{3+}(1000, 1500 ppm)*

		Membrane permeance to each ion [µm·s-1]					
		Al_1900_pH_1			Fe_2000_pH_1		
		[Al +3]	[SO4 -2]	[Ions]	[Fe +3]	[SO4 -2]	[Ions]
Bivalent [+2]	Zinc	56.08	196.28	137.66	17.24	60.33	28.75
	Calcium			848.43			33.34
	Copper			132.53			32.88
Trivalent [+3]	Lanthanum			82.40			27.41
	Praseodymium			84.31			27.67
	Neodymium			83.16			27.00
	Samarium			83.32			27.49
	Ytterbium			72.74			22.85
	Dysprosium			79.31			26.56

Table 4.6: *Dominant salts and trace ions permeance, Fe^{3+}(2000 ppm) and Al^{3+}(1900 ppm)*

4.2 Impact of dominant salts on the removal of trace ions

4.2.1 Majority trace ions rejections, Zn^{2+}, Cu^{2+} and Cu^{2+}

Trace cations of calcium, copper and zinc were added in the solution in order to study their rejections under the influence of $Fe_2(SO_4)_3$ and $Al_2(SO_4)_3$. On average, the ionic rejections in both scenarios had the same tendency although there were important variations. As listed in table 4.7, the solute rejections of majority trace ions follow as Zn^{2+}>Cu^{2+}>Ca^{2+}, however the rejections improved when ferric sulphate was the dominant salt.

OBSERVABLE REJECTION		pH 1							pH 1.5
		Al_300	Al_600	Al_1800	Fe_500	Fe_1000	Fe_1500	Fe_2000	Al_600
Bivalent [2]	Sulphate	15 %	12 %	23 %	21 %	24 %	27 %	33 %	20 %
	Calcium	18 %	7 %	18 %	21 %	22 %	24 %	28 %	12 %
	Copper	19 %	12 %	16 %	22 %	24 %	26 %	26 %	15 %
	Zinc	20 %	13 %	17 %	23 %	30 %	30 %	29 %	14 %
Trivalent [3]	Aluminium	41 %	31 %	31 %	46 %	47 %	53 %	57 %	31 %
	Iron	-	-	-	37 %	36 %	42 %	45 %	-
	Dysprosium	29 %	21 %	20 %	32 %	39 %	35 %	29 %	22 %
	Lanthanium	27 %	20 %	18 %	30 %	34 %	33 %	27 %	21 %
	Neodymium	26 %	19 %	18 %	29 %	37 %	33 %	27 %	20 %
	Praseodymium	26 %	19 %	17 %	29 %	36 %	32 %	27 %	20 %
	Samarium	26 %	19 %	17 %	29 %	36 %	32 %	27 %	20 %
	Ytterbium	30 %	21 %	20 %	34 %	41 %	37 %	31 %	22 %

Table 4.7: *Maximum rejections for ions traces at different conditions of dominant salt*

Considering DiE as the main exclusion mechanism besides cations repulsion at membrane surface, is possible to explain this apparent lack of correlation between the outcomes. At pH 1, zinc forms only one specie with sulphate $Zn(SO_4)_4^{6-}$ as shown in figure 4.11a, while copper and calcium form neutral complexes (as shown in figure 4.11b and 4.11c). Therefore, in NF, neutral species have insignificant interactions with the CM. Consequently, calcium cation, bisulphate calcium $CaHSO_4^+$ in addition to zinc complex are rejected as followed R($Zn(SO_4)_4^{6-}$)>> Ca^{2+}=Cu^{2+}>$CaHSO_4^+$, under DiE exclusion. Adding to that, the notable effect of $Zn(SO_4)_4^{6-}$ shielding with membrane positive charge as to balance the global

electrostatic repulsion.

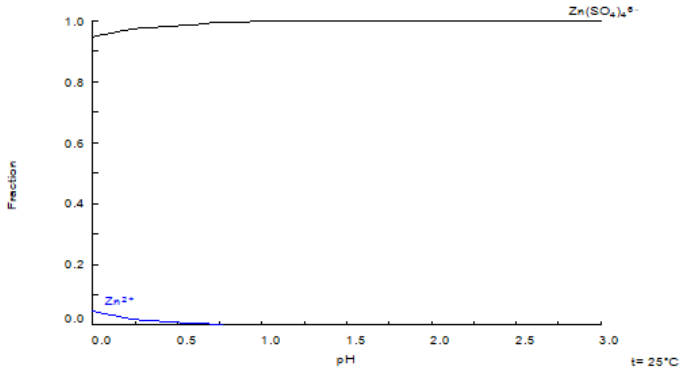

(a) *Zinc speciation diagram*

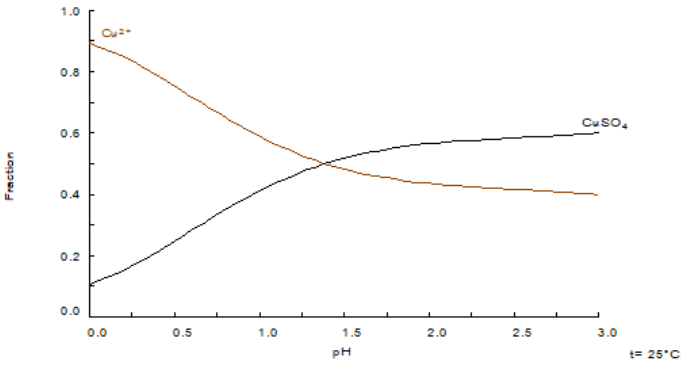

(b) *Copper speciation diagram*

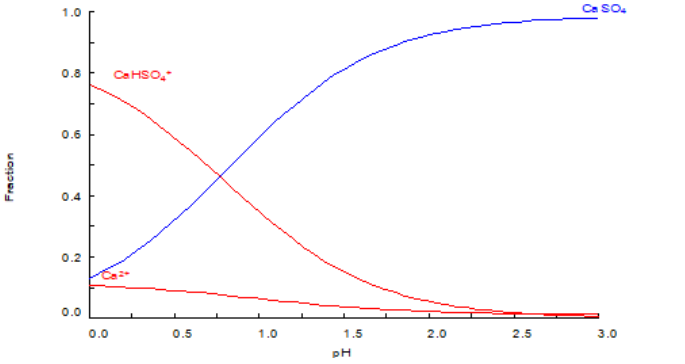

(c) *Calcium speciation diagram*

Figure 4.11: *Majority trace ions speciation diagrams*

4.2.2 Rare earth element or minority traces ions rejections

The application of CM in NF is relatively a new technology in filtration and their demand is growing exponentially. However, using them for REE recuperation is still under investigation and was an interesting aspect in this project since these elements have an important value in

different industrial applications. The rejection of REE for all the performances are detailed in table 4.7. Contrary to expected, REEremoval were lower but in fact improved under certain conditions and were slightly better rejected than the majority of the trace ions. As introduced in the experimental methodology, their concentration were maintained at a nominal value of 10 ppm for all experiment under the influence of aluminium and ferric sulphate. Generally, REE speciation environment is quite similar for each element, as the element M represents them in figure 4.12. From this diagram, M^{3+}, $MSO_4{}^+$ and $M(SO_4)_2{}^-$ can be listed as main REE complexes. Therefore, the primary factor in REE rejection is their trivalence which generally amplify the effect of DiE and DE during their transport through the membrane. Consequently, the individual rejection sequence follow as $R(M^{3+}) >> MSO_4{}^+ > M(SO_4)_2{}^-$. Ytterbium was the most rejected at pH 1 when ferric concentration was 1000 ppm, 41%, (table 4.7). From other point of view, REE were expected to be rejected at almost 100% due to their relevant molecular weight and size comparatively to the others elements present in the solution. Therefore, the results did not match with this hypothesis but rather confirmed the influence of ions valence in NF technique using CM.

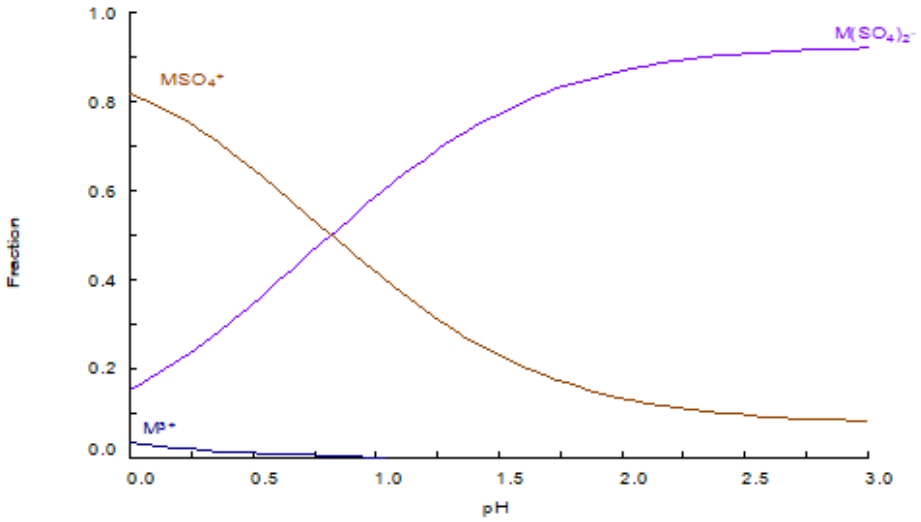

Figure 4.12: *REE speciation diagram where M represents any of the REE investigated in this study*

4.3 Comparison of sulphate salt rejections in AMD with ceramic and polymeric NF membranes

As it has been mentioned, the applications of NF falls in two fields, waste-water treatment and water purification. Also, AMD is a potential threat to the environment that need to be solved. However, the applications of NF membranes on AMD can be achieved with CM which is the main study in this project; and polymeric membrane. Recent studies, reported by Wadekar et al. [25], with CM have proved flexible performance in waste-water from abandoned coal-mine drainage. It compares the performance of NF NF270 polymeric and CM membranes for AMD treatment with a composition reported in (figure 4.13).

Ions	Concentration
Sulfate (mg/L)	645.9 ± 2.5
Chloride (mg/L)	97.8 ± 1.9
Sodium (mg/L)	108.9 ± 4.2
Calcium (mg/L)	151.8 ± 2.1
Magnesium (mg/L)	29.7 ± 1.1
Potassium (mg/L)	4.3 ± 1.6
Manganese (mg/L)	1.2 ± 0.6
Strontium (mg/L)	1.7 ± 0.3
Barium (µg/L)	76.7 ± 4.1
Aluminum (µg/L)	50.5 ± 1.2
Nickel (µg/L)	38.5 ± 4.9
Arsenic (µg/L)	70.0 ± 6.4
Selenium (µg/L)	55.2 ± 3.9
Total iron (mg/L)	< 0.02
pH	7.8 ± 0.2

Figure 4.13: *Composition of the AMD, used by Wadekar et al. [25] for the treatment with polymeric and ceramic NF membranes*

Therefore, the experiments were characterized by ionic retention and permeability as a function of permeate recovery rates. The impact of permeate recovery on ionic rejection and permeability of both membranes was tested with real AMD at recoveries of up to 75% as shown in (figure 4.14 and 4.15).

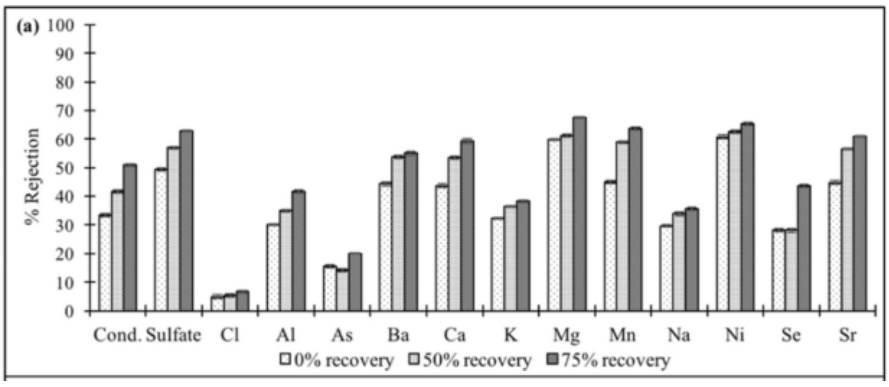

Figure 4.14: *Ionic rejection at different permeate recovery for ceramic membrane, [25]*

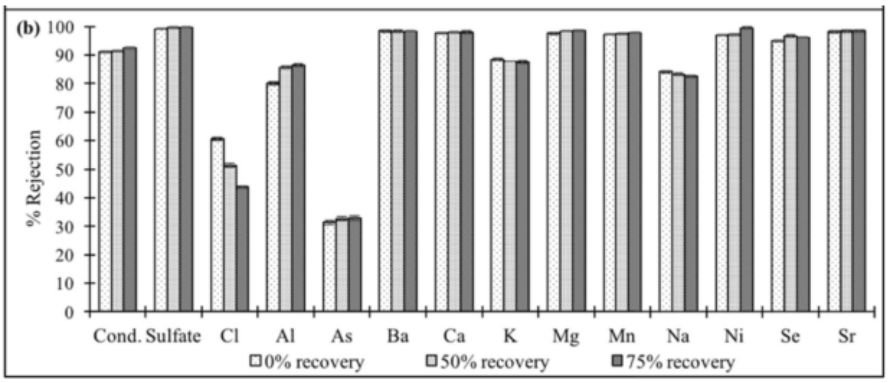

Figure 4.15: *Ionic rejection at different permeate recovery for polymeric membrane NF270, [25]*

The ionic rejection increased with an increase in permeate recovery, with NF270 membrane achieving higher rejection than the ceramic membrane for all ions under all experimental conditions. NF270 membrane rejection were superior to 96% for all multivalent ions as reported in 4.15 while the ceramic membrane achieved rejections between 55 and 67%, as reported in 4.14. Arsenic was not effectively rejected by either membrane (NF270 achieved 33% and ceramic membrane achieved 20%), [25]. Comparatively to the results of this project, the rejections of sulphate and traces ions performed by both CM are still lower in comparison with polymeric NF20 membrane. Nevertheless, CM are potentially strong in extreme conditions, but still need important improvement in order to acquire higher rejections as polymeric membranes.

4.4 Hydraulic permeability

One of the most important measures for the characterization of the transport in filtration is Kw, which was calculated in this study using equation (3.3). As stated, Kw describes the easiness with which a fluid (usually water) can move through pore spaces of the membrane. This section aims to discuss the influence of the dominant salt composition on CM Kw and permeate flux. The permeate flux calculated with equation (3.2) varies linearly with TMP, and the Kw represents the slope. For instance, as shown in figure 4.16, the blue and orange dots are permeate flux at different TMP and pH. Therefore, it can project any variation in experimental conditions so that it was used to give strength to variation in dominant salt compositions. For example, the minimum pressure required for permeation can be observed at the intersection between TMP axis and flux line. Furthermore, the permeabilities can be used to evaluate qualitatively at first sight the cleaning task required to recovery pre-experimental conditions. The inferior limit, for the membrane Kw during the project was approximatively 9 $\mu m \cdot s^{-1} \cdot bar^{-1}$.

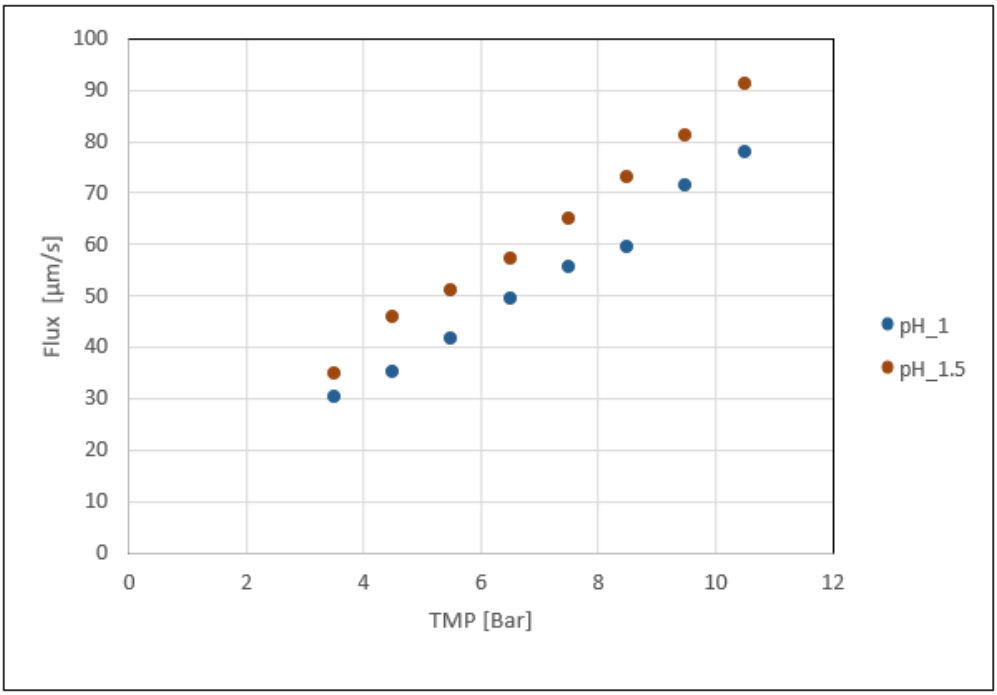

Figure 4.16: *Flux and Kw variation at different pH*

4.4.1 Impact of dominant salt $Al_2(SO_4)_3$ and $Fe_2(SO_4)_3$ present in the feed solution

The impact of aluminium concentration in $Al_2(SO_4)_3$ solutions is shown on permeate flux representation in figure 4.17. As expected the Kw values would increase as aluminium and sulphate concentration decreases. However the results did not confirm that but indicated another case. Firstly, Kw tended to increase along with aluminium concentration at lower solute rejections. Secondly, aluminium speciation showed to be linked to sulphate concentration. Therefore depending on the species in place, the membrane fouling can be more important followed by a flux decrement. For example an important fouling occurs at 300 ppm where $Al(SO_4)_2^-$ in order to maintain electro-neutrality increase the contact with CM free volume. Adding to that, despite the important differences between 600 and 1900 ppm of aluminium, there is not an important increment in permeabilities and Kw stayed at approximatively at 7 $\mu m \cdot s^{-1} \cdot bar^{-1}$.

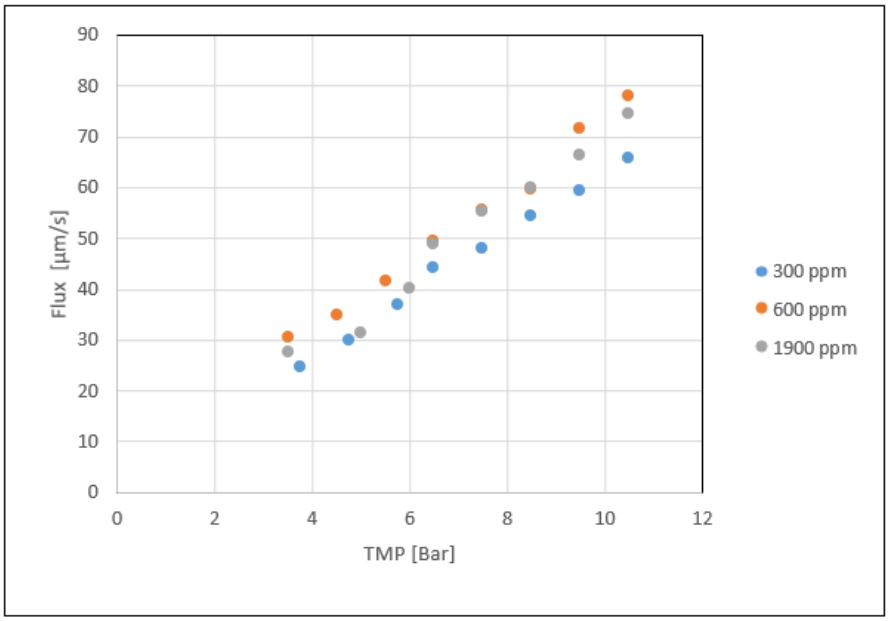

Figure 4.17: *Flux variation for $Al_2(SO_4)_3$ dominant salt at different concentration of aluminium*

Moreover figure 4.18 depicts the impact of ferric concentrations on $Fe_2(SO_4)_3$ solutions and Kw.

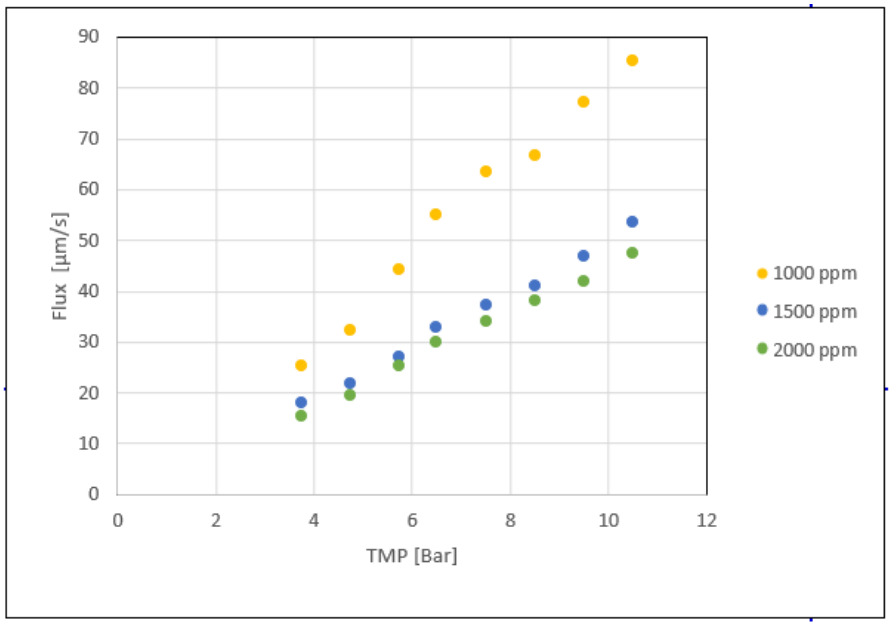

Figure 4.18: *Flux variation for dominant salt $Fe_2(SO_4)_3$ at different concentrations of iron(III)*

Conversely to aluminium ions, ferric ions have an important effect on Kw and CM permeate flux. Clearly, the increase of ions concentration generates a severe decrement in Kw,

8.0, 5.0 and 4.5 $\mu m \cdot s^{-1} \cdot bar^{-1}$ at 1000, 1500 and 2000 ppm respectively. That consequently produces an important flux reduction. For example, permeate flux drastically decrease from 1000 to 1500 ppm as shown in figure 4.18 and therefore still decrease at 2000 ppm. This remarkable observation indicates that fouling phenomenon is most important with iron(III) than aluminium cations. Mainly, because of ferric sulphate speciations, and their intense electrostatic pressure in the CPL which inherently conducts to a severe inorganic fouling.

In order to evaluate membrane fouling, filtration experiments were carried out for 24 h in total recirculation mode while monitoring the transient permeability similar to Kw. For that experimental condition, the measurement was done in LMH/bar which is convenant for large instalations. So, figure 4.19 shows the measurements for the ceramic and NF270 membranes at different permeate recoveries. The maximum decrease in transient permeability was observed at 75% recovery for both membranes. As result, the permeability of the CM decreased by 13.6% (from 0.81 LMH/bar to 0.70 LMH/bar, figure 4.19a), and decreasing by 16.2% (from 8.78 LMH/bar to 7.36 LMH/bar, figure 4.19b) for NF270. Therefore, the increment in rejection with a decrement in permeability suggests that scaling/fouling has occurred in these tests and can suggest the adequate moment for a cleaning operation [25]. These evidences also demonstrate the long-term resistance of CM even if the permeate flux was lower for this experimental set up.

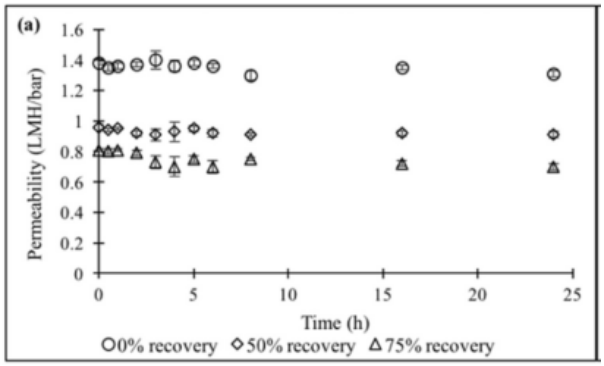

(a) *Permeability at different permeate recovery for ceramic membrane*

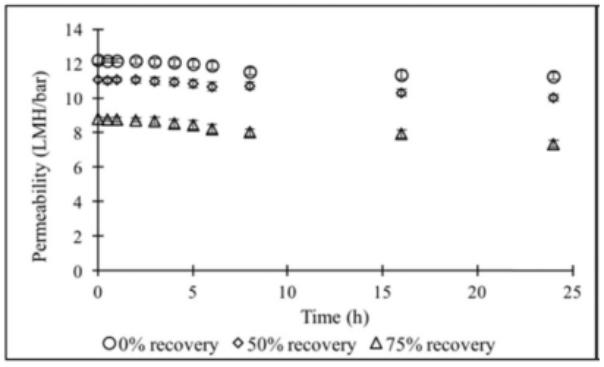

(b) *Permeability at different permeate recovery for polymeric membrane NF270*

Figure 4.19: *Permeability at different permeate recovery for ceramic and polymeric membrane, [25]*

Chapter 5

COSTS EVALUATION

Despite the different approximation used for the economic evaluation, any project should be able to reflect the fund necessary, for execution. That is to say, that the cost estimation was an important features in this study. It was done by including different factors which are detailed in this section. Firstly, the installation cost that permits to run all the experiments is presented after the evaluation of depreciation rate. The costs of the equipments have been estimated using equation (5.1) and the results are presented in table 5.1, and besides the cost of the analytical techniques were also included.

$$\text{Amortization Cost} = \frac{Equipment\,Cost}{Lifetime} \cdot \mathrm{t_{use}} \tag{5.1}$$

where:
$\mathrm{t_{use}}$: is the time of use of the equipment, in year.

Installation	Use [year]	Units [u]	Amortization rate [€/year]	Lifetime [year]	Cost [€]
Hydra-Cell G10	0.3	1	452.00	8	135.60
Tank 30 L	0.3	1	23.17	8	6.95
Thermostat DIGIT-COOL	0.3	1	60.35	8	18.11
PVC Tube	0.3	3	0.46	5	0.14
SS-316 Tubre	0.3	4	2.25	8	0.68
By-pass Valve	0.3	1	33.60	8	10.08
Valve	0.3	1	9.78	8	2.93
Flowmeter	0.3	1	59.38	8	17.81
Manometer	0.3	2	1.25	8	0.38
Catridge Filter	0.3	1	5.10	1	1.53
Filter enclosure	0.3	1	3.39	5	1.02
Membrane module	0.3	1	21.07	8	6.32
Ceramic: 10 NM TIO2 - SG 2055-A	-	1	-	-	126.50
				Total	328.04 €
Analytical technique	**Use [year]**	**Units [u]**	**Amortization rate [€/year]**	**Lifetime [year]**	**Cost [€]**
pH-meter	0.3	1	37.06	8	11.12
Conductivity-meter	0.3	1	56.12	8	16.83
Precision mass balance	0.3	1	13.49	8	4.05
ICP	-	-	-	-	1260.00
				Total	1,292.00 €

Table 5.1: *Installation and analytical technique costs estimation*

Table 5.2, presents all the reagent used for the project including their cost.

Reagent	Quantity [kg]	Price[€/Kg]	Cost [€]
$Al_2(SO_4)_3 \cdot 18H_2O$	6.97E-01	27	18.82
$Cu(SO_4) \cdot 5H_20$	5.18E-03	63	0.33
$Ca(SO_4) \cdot 2H_2O$	5.58E-03	101.6	0.57
$FeSO_4 \cdot 7H_2O$	2.86E-01	24.8	7.09
$Zn(SO_4) \cdot 7H_2O$	5.82E-03	50.1	0.29
$La_2(SO_4)_3 \cdot 9H_2O$	1.42E-03	3064	4.35
$NaOPr \cdot 6H_2O$	1.68E-03	4310	7.24
$NdCl_3$	9.40E-04	3012	2.83
$Sm(NO_3)_3 \cdot 6H_2O$	1.60E-03	27200	43.52
Dy_2O_3	6.20E-04	4620	2.86
Yb_2O_3	6.20E-04	6120	3.79
H_2O_2	0.5	32 €/L	16.00
H_2SO_4	0.2	32 €/L	6.40
		Total	114.10 €

Table 5.2: *Reagents costs estimation*

Two types of water were used. Table 5.3 presents the cost of water supply and also includes the cost of power consumption.

Water	Quantity [L]	Price [€/L]	Cost [€]
Milli Q	10	2.8	28.00
Supply	621	0.55	341.55
		Total	369.55 €
Power supply	**hour [hr]**	**Price [€/Kwh]**	**Cost [€]**
Pump	100	0.6	60.00
		Total	60.00 €

Table 5.3: *Power and water supply costs estimation*

Any of these studies can not be performed without the technical knowledge required. Two groups of human resources were needed. Firstly, the technicians whose main job was the execution of all the operatives tasks and secondly, the supervisors, who revised and guided the project. An overview on the cost of labour is shown in table 5.4.

Laboratory	Units [u]	Price [€/u]	Cost [€]
Glove	20	2.5	50.00
Protection Glasses	1	5.95	5.95
Lab-coat	1	22.43	22.43
Micropipette tips	5	4.35	21.75
Micropipette 100-1000 µL	1	28.5	28.50
Micropipette 1-10 mL	1	28.5	28.50
Others	-	-	100.00
		Total	257.13 €
Labour	**Hour [hr]**	**Cost of labour [€/hr]**	**Cost [€]**
Supervisor	75	40	3000.00
Bibliographic research	75	15	1125.00
Experiment	100	15	1500.00
Data analysis	200	15	3000.00
Writting	250	15	3750.00
		Total	12,375.00 €

Table 5.4: *Labour and laboratory activities costs estimation*

Finally, table 5.5 presents the global cost and the different items used for the economic evaluation.

Items	
Installation	328 €
Analytical technique	1,292 €
Reagent	114 €
Water	370 €
Power supply	60 €
Laboratory	257 €
Labour	12,375 €
Total	14,796 €

Table 5.5: *Global cost estimation of the project*

Chapter 6

ENVIRONMENTAL IMPACT

Since human actions have both positive and negative impacts on the environment, the environmental impact analysis refers to the study of the alterations induced by human actions. This section will expose the impacts generated using a laboratory scale NF plant, and including all the activities related to the applications on AMD. The efforts focused on the evaluation and the identification of different positive and negative consequences. Consecutively, the actions implemented have the aim to eliminate or reduce the negative, and maximize the positive impact. The items analysed are related to the operations needed to run the plant, the experiments carried out and finally the analysis and manipulation of samples generated during the project.

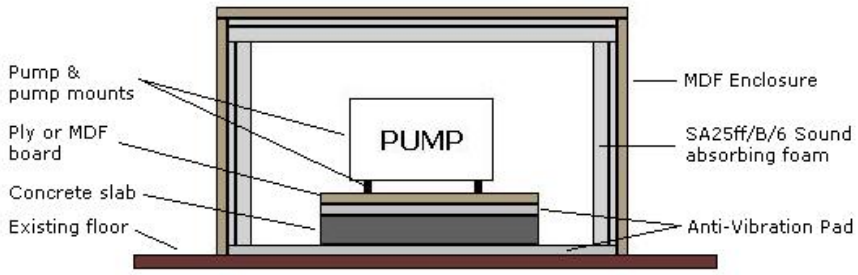

Figure 6.1: *Pump protection with anti-noise and vibration box, schematic*

Regarding the analysis of the plant, only the activities related to the operations are taken into account, as the installation was built before this project and had been used in the past for others similar activities. The use of the installation starts by running different types of operation enumerated in the experimental methodology. In general, the electric energy consumption was a clear fact, and consequently is related to the emission of pollutants somewhere in the planet. So, the use of the motor pump and the refrigeration system were planned to avoid overconsumption.

Adding to that, around the nearest environment to the plant, other negative impacts were created. For instance, the noises and the vibrations that occur during the motor pump operations. However, in order to minimize these two factors, the pump has been enclosed inside an anti-noise and vibration enclosure, following the installation procedure, as illustrated in figure 6.1. A closer observation to figure 6.2, can help to identify these parts comparatively

to figure 6.1. The box filled with noise-absorbent material in the ground, and also beneath the pump, an anti-vibrating installation can be observed. This installation reduces considerably the noise and the vibration during the experiments. Nevertheless, the ideal case of a noiseless environment cannot be achieved due to the physical limitations of the installation. Another important point, is the heat generated when the motor pump is running. That can be demeaned by closing the protection box or opening the windows of the laboratory.

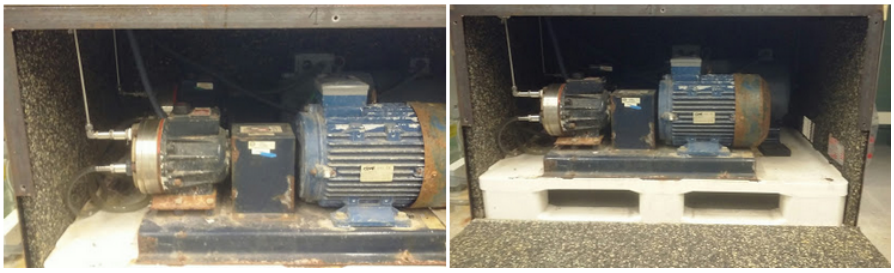

Figure 6.2: *Pump protection with anti-noise and vibration box, installation*

The experimental work requires different solutions, such as acidic solutions; potable water; synthetic solutions with a mixture of different family of reagents. Therefore, they were necessary to simulate AMD with different parameters and characteristics. From the environmental friendship view, all that activities and products manipulation need a strict precaution procedure as to avoid contamination. Moreover, as the project has a clear purpose to reduce the negative impact of AMD on the environment, it was important to have always in mind the reduction of leaking from these solutions. That was achieved by storing them in a stable plastic container, then avoiding the exposure to the ambient and describing as well their composition. Furthermore any filtration in the sewers were avoided as to minimize contamination with heavy metals and an important fact is the use of large quantity of potable water. Approximately, 621 L of water were used for all the experiments. That was inevitable, due to the requirements of the study. However, it was considered as an investment to improve water quality using NF technique in the future. Finally, the sample analysis required different laboratory task where different types of material had been used. For that reason, many recycling habits were applied such as solutions recycling, plastic recycling and also paper recycling. Different aspects of these impacts and their description is shown in table 6.1.

Aspect	Description
Emissions and discharges	Liquid or gas substances that are disposed of into the environment
Noise pollution	Sound and vibrations produced by the equipment
Resource consumption	Consumption of electricity, fuel and water
Products and by-products	Chemical products produced by the plant
Waste	Management of waste products produced by the plant

Table 6.1: *Negatives environnemental impact related to the plant operations, [26]*

Chapter 7

CONCLUSIONS

The present study on NF using CM, was limited to the different objectives previously stated. So, after the analysis of the performances is possible to resume the conclusions as following:

- The rejection of sulphate apparently increased with aluminium concentration, the results were 15%, 12% and 23% respectively at 300, 600 and 1900 ppm of aluminium. Despite, these rejections are still low comparatively to other applications, they permit to understand the relationship between sulphate speciation with aluminium and the behaviour of the CM, at least on exclusion and transport mechanisms.

- The rejection of sulphate has increased from 12% to 20% when pH was shifted from 1 to 1.5, when the dominant salt was $Al_2(SO_4)_3$. That can be explained with the H^+, $HSO_4{}^+$ and $SO_4{}^{2-}$ equilibrium, which justifies the increment of $HSO_4{}^+$ fraction at pH 1. However, $HSO_4{}^+$ is clearly less rejected than $SO_4{}^{2-}$ due to dielectric exclusion. It will be, useful in the future to plan a new strategy to highlight the real interaction between aluminium and iron with sulphate salts at different pH. Then, sulphate elimination can be improved considerably in acidic conditions.

- Comparatively to the rejections of sulphate obtained with aluminium, the addition of ferric ions improved the expected rejection from 15% to 21%. After the examination of $Al_2(SO_4)_3$ speciation with the addition of Fe^{3+}, it was clear that the increment in iron complexes reduce the fraction of $HSO_4{}^+$ that reduced the membrane global permeability to sulphate ions. Consequently, is possible to admit that the presence of iron have an important influence on sulphate speciation which indirectly, can be used to harness the rejection of sulphate in acidic conditions.

- Clearly the rejection of sulphate under the influence of ferric sulphate as dominant salt yields the best results in these conditions. The rejections were 24%, 27% and 33% respectively at 1000, 1500 and 2000 ppm of iron. Here again, sulphate speciation with ferric ions was important for these performances. The formed species were more sensible to Donnan and dielectric exclusions, consequently their interaction with the membrane was notable. However, their accumulation inside the membrane create important fouling, which potentially reduces the hydraulic permeability. All in all, the presence of iron in AMD solution can be used as important factor when using CM and the improvements to

reduced fouling can create some useful applications.

- Generally, the solute rejection of trace ions depends firstly on the rejection of dominant ions and secondly on their speciation with sulphate. Clearly, there is a great difference between bivalent and trivalent ions rejection. Apparently, in all cases trivalent ions were more rejected than bivalent ones or at least they show to interact intensively with the membrane. However, zinc and ytterbium the most rejected elements presented different behaviours. Inside the bivalent group, zinc rejection was higher, 30% , when the concentration of iron(III) was 1000 ppm as well as Ytterbium, 41%, for trivalent group. Therefore, when ferric concentration increased trivalent ions rejection tend to decrease while the rejection of bivalent ions remains constant. For example, zinc yields 30%, 29% against 37% and 31% for Ytterbium at respectively 1500 and 2000 ppm. Also, the ions permeabilities show to decrease considerably with the presence of iron. All that said, is possible to summarize that, ferric ions has a rejection impact higher than aluminium and for the applications with AMD.
- Finally, SDFM modelling proved to be useful for NF applications using CM, specially when there is a clear dominant salt. It permits to calculate with accuracy the membrane permeabilities to each ions in all scenarios and made easier the interpretation and visualization of the experimental data.

List of Figures

List of Tables

Bibliography

[1] Ata Akcil and Soner Koldas. Acid Mine Drainage (AMD): causes, treatment and case studies. *Journal of Cleaner Production*, pages 1139–1145, Volume 14 - 2006.

[2] Geoffrey S. Simate and Sehliselo Ndlovu. Acid mine drainage: Challenges and opportunities. *Journal of Environmental Chemical Engineering*, pages 1785–1803, Volume 2 - 2014.

[3] Trevor Chase and George Sparks. Filters and Filtration Handbook. pages 55–111. Ltd., Elsevier, Edition 6 - 2008.

[4] Vitaly Gitis and Gadi Rothenberg. Ceramic Membrnaes New Opportunities an Practical Applications. pages 149–268. John Wiley and Sons, Edition 1 - 2016.

[5] Roy Yagnaseni, David M. Warsinger, and John H. Lienhard. Effect of temperature on ion transport in nanofiltration membranes: Diffusion, convection and electromigration. *Desalination*, pages 241–257, Volume 420 - 2017.

[6] Andrij E. Yaroshchuk. Dielectric exclusion of ions from membranes. *Advances in Colloid and Interface Science*, pages 193–230, Volume 85 - 2000.

[7] Seong Jik Park, Ravi Kumar Cheedrala, Mamadou S. Diallo, Changmin Kim, In S. Kim, and William A. Goddard III. Nanofiltration membranes based on polyvinylidene fluoride nanofibrous scaffolds and crosslinked polyethyleneimine networks. *Nanotechnology for Sustainable Development*, pages 33–46, Edition 1 - 2014.

[8] Neus Pages, Andriy Yaroshchuk, Oriol Gibert, and Jose Luis Cortina. Rejection of trace ionic solutes in nanofiltration: Influence of aqueous phase composition. *Chemical Engineering Science*, pages 1107–1115, Volume 104 - 2013.

[9] Hiroyuki Suda and Kenji Haraya. Molecular sieving effect of carbonized kapton polyimide membrane. *Journal of the Chemical Society, Chemical Communications*, pages 1179–1180, Volume 3 - 1995.

[10] Peter Kosiol, Björn Hansmann, Mathias Ulbricht, and Volkmar Thom. Determination of pore size distributions of virus filtration membranes using gold nanoparticles and their correlation with virus retention. *Journal of Membrane Science*, pages 289–301, Volume 533 - 2017.

[11] Sudipta Sarkar, Arup K. SenGupta, and Prakhar Prakash. The donnan membrane principle: Opportunities for sustainable engineered processes and materials. *Environmental Science and Technology*, pages 1161–1166, Volume 44 - 2010.

[12] Smart membrane Solutions. https://www.smartmembranesolutions.co.nz/membrane-classifications/. Accessed: 2018.

[13] Darren L. Oatley-Radcliffe, Matthew Walters, Thomas J. Ainscough, Paul M. Williams, Abdul Wahab Mohammad, and Nidal Hilal. Nanofiltration membranes and processes: A review of research trends over the past decade. *Journal of Water Process Engineering*, pages 164–171, Volume 19 - 2017.

[14] Woei Jye Lau and Ahmad Fauzi Ismail. Nanofiltration Membranes. pages 1–184. Group, Taylor & Francis, Edition 2017.

[15] Marianne Nyström, Lena Kaipia, and Susana Luque. Fouling and retention of nanofiltration membranes. *Journal of Membrane Science*, pages 249–262, Volume 98 - 1995.

[16] Slide player. https://slideplayer.com/slide/9471279/. Accessed: 2016.

[17] Ken Sutherland. Filters and Filtration Handbook. pages 41–92. Ltd., Elsevier, Edition 5 - 2008.

[18] Technology report. http://technologyreport.mecadi.com/Chapter_2_Gas_separation_with_membranes.php. Accessed: 2008.

[19] Joerg Balster. Spiral wound membrane module. In *Encyclopedia of Membranes*, pages 1–3. Springer Berlin Heidelberg, 2015.

[20] Tim Van Gestel, Carlo Vandecasteele, Anita Buekenhoudt, Chris Dotremont, Jan Luyten, Roger Leysen, Bart Van Der Bruggen, and Guido Maes. Salt retention in nanofiltration with multilayer ceramic TiO2membranes. *Journal of Membrane Science*, pages 379–389, Volume 209 - 2002.

[21] Jeonghwan Kim and Bart Van Der Bruggen. The use of nanoparticles in polymeric and ceramic membrane structures: Review of manufacturing procedures and performance improvement for water treatment. *Environmental Pollution*, pages 2335–2349, Volume 158 - 2010.

[22] W. Richard Bowen and Haitham N.S. Yousef. Effect of salts on water viscosity in narrow membrane pores. *Journal of Colloid and Interface Science*, pages 452–457, Volume 264 - 2003.

[23] Jianquan Luo and Yinhua Wan. Effects of pH and salt on nanofiltration-a critical review. *Journal of Membrane Science*, pages 18–28, Volume 438 - 2013.

[24] Daniel Léon de la Cruz. TFG: Tratamiento de aguas ácidas de mina mediante el uso de una membrana cerámica. pages 1–114, EEBE UPC 2018.

[25] Shardul S. Wadekar and Radisav D. Vidic. Comparison of ceramic and polymeric nanofiltration membranes for treatment of abandoned coal mine drainage. *Desalination*, pages 135–145, Volume 440 - 2018.

[26] Bartomeu Servera. TFG: Acid mine drainage treatment by nanofiltration membranes : impact of aluminium and iron concentration on membrane performance. pages 1–74, ETSEIB UPC 2017.